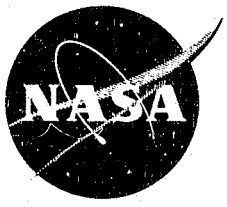

Final Report

INVESTIGATION OF EARTH'S ALBEDO USING SKYLAB DATA

ROBERT E. TURNER
Infrared and Optics Division

JANUARY 1976

Prepared for

NATIONAL AERONAUTICS AND SPACE ADMINISTRATION

Lyndon B. Johnson Space Center
Houston, Texas 77058
Contract No. NAS9-13279
Technical Monitor: Z. H. Burns

ENVIRONMENTAL
RESEARCH INSTITUTE OF MICHIGAN
FORMERLY WILLOW RUN LABORATORIES, THE UNIVERSITY OF MICHIGAN
BOX 618 • ANN ARBOR • MICHIGAN 48107

TECHNICAL REPORT STANDARD TITLE PAGE

1. Report No.	2. Government Accession No.	3. Recipient's Catalog No.
102200-20-F		

4. Title and Subtitle	5. Report Date
INVESTIGATION OF EARTH'S AEROSOL ALBEDO USING SKYLAB DATA	November 1975
	6. Performing Organization Code

7. Author(s)	8. Performing Organization Report No.
Robert E. Turner	102200-20-F

9. Performing Organization Name and Address	10. Work Unit No.
Environmental Research Institute of Michigan Infrared and Optics Division P.O. Box 618 Ann Arbor, Michigan 48107	11. Contract or Grant No. NAS9-13279
	13. Type of Report and Period Covered Final Report
12. Sponsoring Agency Name and Address Lyndon B. Johnson Space Center National Aeronautics and Space Administration Houston, Texas 77058	14. Sponsoring Agency Code

15. Supplementary Notes

Technical Monitor was Z.H. Byrns

16. Abstract

The purpose of this report is to investigate the albedo of the Earth-atmosphere system and, in particular, to determine the feasibility of using satellite sensors to monitor the change in the aerosol content of the atmosphere.

Specific test sites in the White Sands, N.M. and Lake Michigan areas were chosen because of their stability and known reflectances. SKYLAB S-192 multispectral data and ERIM aircraft multispectral data were collected for these sites and were compared with the results of atmospheric-radiative-transfer calculations in order to determine the aerosol content of the atmosphere. The spectral shape of the SKYLAB data compared quite favorably with the nearly simultaneous spectral character of the aircraft data.

Although there were difficulties in the calibration of the S-192 instrument which remain unresolved, interesting mathematical and physical relationships were discovered in this investigation which will allow future investigations to be more meaningful in their information content regarding the albedo of the Earth-atmosphere system.

17. Key Words		18. Distribution Statement
Albedo	Climatology	Distribution is listed at the end of this document
Aerosol	Radiative-Transfer	
Particulates	Atmospheric Model	
Scattering		

19. Security Classif. (of this report)	20. Security Classif. (of this page)	21. No. of Pages	22. Price
UNCLASSIFIED	UNCLASSIFIED	82	

PREFACE

The determination of the albedo of Earth is currently of considerable interest to atmospheric scientists, meteorologists, and global climatologists.

The purpose of this study was to investigate the role of particulates in the atmosphere and in what way they contribute to the albedo of the Earth-atmosphere system, making use of SKYLAB data acquired over specific test sites.

The SKYLAB data and auxiliary aircraft data were analyzed and compared with results of calculations based upon current atmospheric-radiative-transfer models.

This work was performed under Contract NAS9-13279 for the National Aeronautics and Space Administration. The author wishes to thank the project monitor, Z. Byrns and his assistant, W.J. Johnson for the many discussions concerning the handling and analysis of data.

ERIM personnel who participated in the technical part of the investigation were Peter Lambeck and Lynn Ziegler. The typing of the report was done by Jan Dixon. The work was performed in the Infrared and Optics Division under the direction of Richard R. Legault; The Principal Investigator was Robert E. Turner.

TABLE OF CONTENTS

TABLE OF CONTENTS (continued)

LIST OF FIGURES

LIST OF FIGURES (continued)

LIST OF TABLES

SUMMARY

In recent years, meteorologists, atmospheric scientists, and applied mathematicians, aided by modern high-speed computers have been able to improve upon the development of atmospheric models. These models of the atmosphere are used to predict future weather patterns over an extended area and they are also used to study the climate over major portions of the Earth for many centuries in the past and on into the future. This latter study, global climatology is more than of academic interest, for it has much to say concerning the quality of life for all mankind.

Besides the ravages of nature such as tornadoes, hurricanes, drought, floods, and other weather-related phenomena, the seemingly subtle changes in the composition of the Earth's atmosphere can have a profound impact upon our existence. The impetus for the present investigation is the concern over the long-term change in the composition of the semi-permanent atmospheric component called the aerosol.

The first part of this report deals with general aspects of radiation balance for the Earth and the development of atmospheric-radiative-transfer models used in the description of the Earth's natural radiation field. The last part of the report deals with the calculations of the Earth's albedo using the models of the atmosphere and the multispectral data obtained by SKYLAB.

2

INTRODUCTION

The temperature of a planet is determined by equating the incoming flux from the sun (multiplied by the fraction of energy absorbed) to the outward radiated flux. The temperature is thus dependent upon the solar flux and the albedo of the planet, where we can define the albedo as the ratio of the reflected radiation to the incident radiation. In this sense, the albedo of the combined atmosphere-surface system is somewhere between zero and unity. If the albedo is zero, the planet absorbs all incident radiation and re-radiates it as thermal radiation. On the other hand, if the albedo of a planet is unity, then none of the incident radiation is absorbed and no temperature can be stated.

The radiation balance of a planet is determined by the solar flux value, the reflectance of the planetary surface, and by the reflectance and absorption properties of the planetary atmosphere. As a result of man's activities such as the large-scale cultivation of the soil, irrigation, and the building of roads and cities, the surface features of Earth have been altered over the years. This has the effect of changing the surface reflectance or albedo. Likewise, man has succeeded in changing the atmosphere by introducing artificial gases and particulates which can change the atmospheric albedo. Although man has no direct influence on the solar flux, it is known that the energy radiated by the sun is not constant in time. All of these effects can change our environment, either in a direct way by allowing a greater or lesser amount of solar radiation to reach the Earth's surface, or in an indirect way by altering those atmospheric conditions which lead to changes in our climate. It is therefore important that we know how rapidly and in what way the planetary albedo of the Earth is changing so that climatologists can improve the predictive capability of their models.

In this report we shall primarily be concerned with the possible variation in the particulate component of the atmosphere. Using radiative-transfer theory, an atmospheric radiation model has been developed which is then used to calculate the spectral albedo of the Earth for a great variety of possible

atmospheric states. Interesting relationships are shown which connect the albedo to easily measurable quantities for various atmospheres and energy conservation relations are defined for any atmospheric state. Finally, using SKYLAB multispectral data for specific target areas we attempt to describe the aerosol contribution to the Earth's albedo. In doing this we clearly point out the difficulties encountered in this method of albedo determination and describe techniques for overcoming such problems in the future.

3

THE ENERGY CYCLE

With the exception of radioactive materials inside the Earth, almost all of the external energy we have comes ultimately from the sun. Energy from the sun is reflected and absorbed by the atmosphere and is reflected and absorbed by the Earth's surface. In this section we shall consider the spectral character of the solar radiation and the terrestrial radiation within realistic atmospheres.

3.1 Solar Radiation

There have been many measurements of the so-called solar constant, i.e., the total energy incident upon the atmosphere integrated over the entire spectrum. Some of the many references to this work over the years is given by Drummond[1] and an excellent history of the measurement of solar radiation is given by Henderson[2]. Most of these investigations however, involving an extrapolation to zero air mass are considered to be unreliable. More recent measurements have been made aboard balloons, high-altitude aircraft and spacecraft by Arvesen et al.[3], and Thekaekara and Drummond[4] which indicate that the earlier values of the solar spectrum were too high. There could be intrinsic fluctuations in the solar spectrum other than the well known large fluctuations in the ultraviolet part of the spectrum. We shall use the NASA standard values given by Thekaekara and Drummond for our analysis. A portion of the spectrum in the near-UV, visible, and near-IR is illustrated in Figure 1. Figure 2 depicts the spectrum according to Pettit[5] over an extended part of the spectrum and it also shows the spectrum at sea level. Nimbus F satellite, launched in the summer of 1975 is providing data on the extra-terrestrial solar spectrum in connection with the Earth Radiation Budget investigation and Nimbus G will also monitor the solar spectrum. As a result of these future satellite measurements, we hopefully will have a more detailed knowledge of the solar spectrum and its variations.

FIGURE 1
NASA STANDARD EXTRATERRESTRIAL
SOLAR SPECTRUM

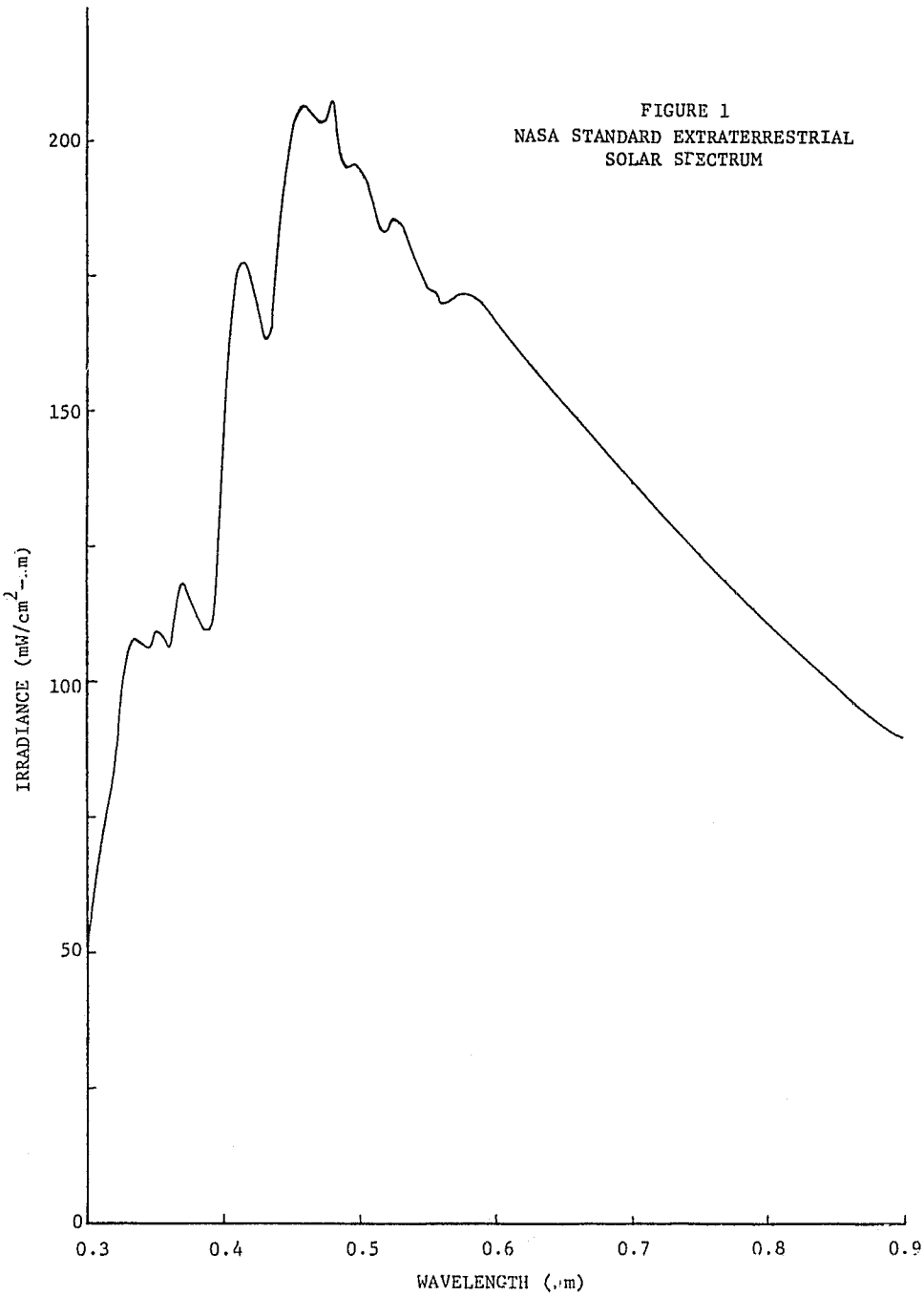

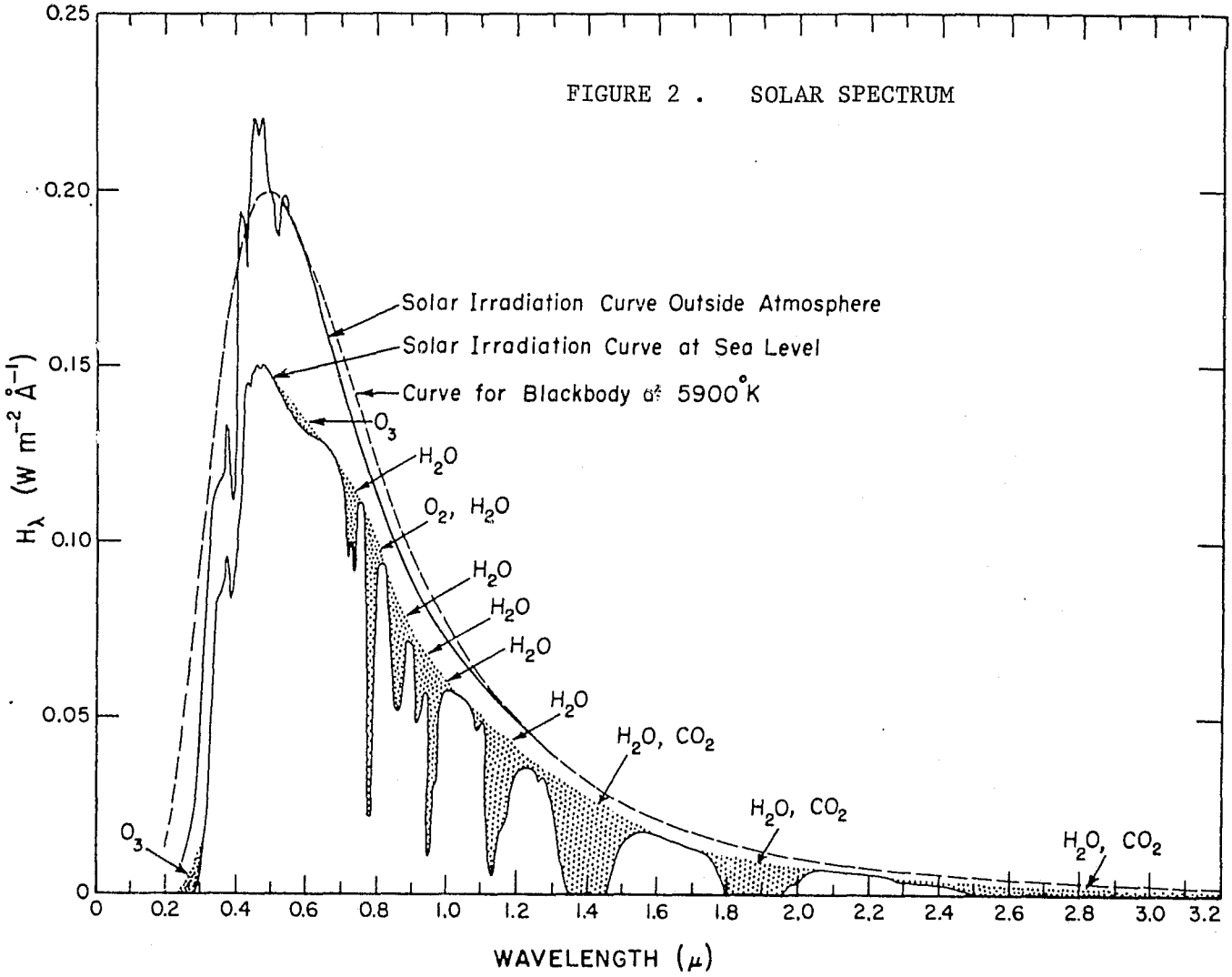

3.2 Atmospheric Structure

In this section, we shall be concerned with the basic structure of the atmosphere insofar as it applies to the problem of the transfer of radiation.

3.2.1 Atmospheric Gases

The Earth's atmosphere consists primarily of molecular oxygen and nitrogen and the atomic gas argon. Variable gaseous components are water vapor, carbon dioxide, ozone, sulfur dioxide, hydrogen sulfite, hydrogen, and other complex molecules such as nitrogen compounds, methane, and formaldehyde. The strongest absorption of radiation by gases takes place

in the ultraviolet and infrared part of the spectrum. Oxygen (O_2), nitrogen (N_2), and ozone (O_3) absorb primarily in the ultraviolet whereas water vapor (H_2O), carbon dioxide (CO_2) and ozone absorb strongly in the infrared. Throughout the visible part of the spectrum, the only significant absorption by gases occurs in Chappuis band of ozone near 0.6μm.

Besides absorbing radiation, gases and small fluctuations in the density of air can also scatter radiation. If the scattering center is much smaller than the wavelength of the incident radiation, then an oscillating electric dipole field is created. Lord Rayleigh calculated this effect almost a century ago and found the angular and spectral dependencies of the radiation to be as follows:

$$\text{Intensity} \propto \lambda^{-4}(1+\cos^2\theta) \qquad (1)$$

where λ is the wavelength and θ is the angle between the incoming and outgoing radiation. This type of scattering is referred to as Rayleigh scattering and is responsible for the blue color of a clear sky. There are, in addition, other scattering processes associated with the interaction of higher energy photons with gases but these are not of interest to us here.

3.2.2 Aerosols

Small particles arising from a great variety of natural and anthropogenic sources can temporarily be suspensed in the atmosphere. This semi-permanent suspension of liquid or solid particles in the atmosphere is called an aerosol. Examples are hazes, clouds, fogs, mists, smoke, smog, and dust. The particles form around a tiny nucleus composed of various organic and inorganic materials such as ammonia, nitrates, sulfates, and hydrocarbons. The sources of aerosols have been summarized by Hidy and Brock[6] and are presented in Table I.

The sizes of particles can vary over a wide range. Junge[7] has divided the aerosols into three categories; Aitken nuclei with radii

TABLE I. SOME IMPORTANT SOURCES OF ATMOSPHERIC AEROSOLS. Production Rate in Tons Day^{-1} on a Worldwide Basis

(a) Natural

Source	Estimated production rate	Max. % by wt. of total
1. Primary		
Dust Rise by Wind	2×10^4-10^5	9.3
Sea Spray	3×10^6	28.
Extraterrestrial (meteoritic dust)	50-550	
Volcanic Dust (intermittent)	10^4	0.09
Forest Fires (intermittent)	4×10^5	3.8
2. Secondary		
Vegetation (hydrocarbons-terpenes)	5×10^5-3×10^6	28.
Sulfur Cycle (oxidation of H_2S—SO_4^{2-})	10^5-10^6	9.3
Nitrogen Cycle		
Ammonia	7×10^5	6.5
NO_X—NO_3^-	10^6	8.3
Volcanoes (volatiles, SO_2 and H_2S) — intermittent	$\sim 10^3$	0.009
Sub-total	10.1×10^6	94.

(b) Anthropogenic

Source	Estimated Production rate	Max. % by wt. of total
1. Primary		
Combustion and industrial	$1\text{-}3 \times 10^5$	2.8
Dust rise by cultivation (intermittent) (U.S. only)	10^2-10^3	0.009
2. Secondary		
Hydrocarbon vapors (incomplete combustion, etc.	7×10^3	0.065
Sulfates (oxidation of SO_2 and H_2S)	3×10^5	2.8
Nitrates (oxidation of NO_X)	6×10^4	0.56
Ammonia	3×10^3	0.028
Sub-total anthropogenic	6.7×10^5	7.1 - 6%
Total: All sources	10.7×10^6 tons day^{-1}	

between 10^{-7} cm and 10^{-5} cm, large particles with radii between 10^{-5} cm and 10^{-4} cm, and giant particles with radii greater than 10^{-4} cm Deirmendjian[8] has considered various mathematical formulas for representing the size distributions. One of these formulas is the so-called modified gamma distribution given by

$$n(r) = ar^{\delta} \exp(-br^{\gamma}) \; ; \; 0 \leq r < \infty \tag{2}$$

where the various parameters of the distribution function are related to the number density and the mode radius of the particles. In Equation (2) n(r) is the number of particles per unit volumes of radius r. Figure 3 illustrates the size distribution functions for haze M (marine or coastal), haze L (continental), and haze H (stratospheric).

For atmospheric optics, the composition of particulates manifests itself in terms of the complex index of refraction. It is represented as follows:

$$m(\lambda) = m_1(\lambda) - im_2(\lambda) \tag{3}$$

where $m_1(\lambda)$ is the real part of the refractive index which is responsible for the scattering of the radiation and $m_2(\lambda)$ is the imaginary part which corresponds to absorption of radiation. To determine the refractive index for an extended region of the atmosphere is not an easy task. Usually in situ sampling is performed and absorption methods are carried out in the laboratory to find the imaginary part. In general, as the amount of water vapor increases the particles have more water in them and the index therefore approaches that corresponding to pure water. Thus, in the visible region $m(\lambda) \rightarrow 1.33$ as the water vapor increases. A more detailed treatment of aerosol absorption is given by Turner [9] for the case of realistic atmospheres.

It is usually assumed that the aerosol particles are spherical in shape. This assumption is probably valid for water or liquid particles but dry particles can have any shape. It is not clear how the non-sphericity affects the optical properties of the particles for a polydispersion, i.e.

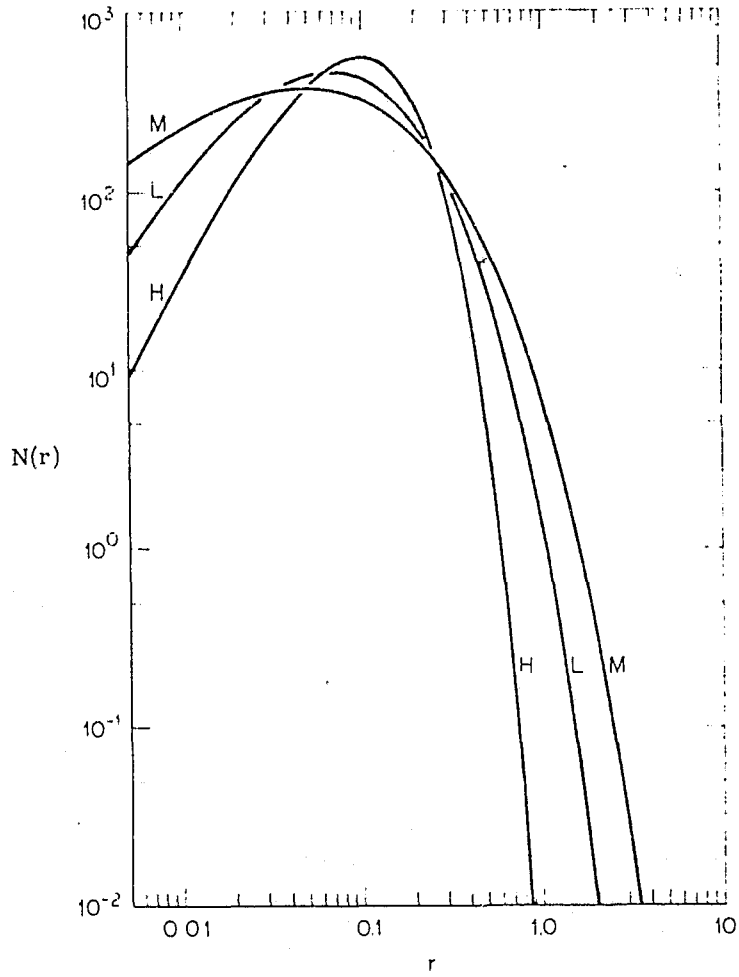

FIGURE 3. HAZE-TYPE DISTRIBUTION FUNCTIONS. The units for the radius r and for the unit volume in N(r) depend on the particular model.

a large collection of particles with a spectrum of sizes. It is commonly assumed that if the particles are of random orientation then the gross optical property is similar to that for a collection of spherical particles.

3.2.3 Attenuation of Radiation

The attenuation of an infinitely narrow monochromatic beam of radiation can be expressed by the following equation:

$$I_\lambda(x) = I_\lambda(0)\exp[-\int_0^x \kappa_\lambda(x')dx'] \tag{4}$$

where $I_\lambda(x)$ is the intensity of the beam at distance x, $I_\lambda(0)$ is the source intensity, and $\kappa_\lambda(x)$ is called the volume extinction coefficient. The extinction coefficient $\kappa_\lambda(x)$ is a measure of the total loss of energy by both absorption and scattering processes along the path. Thus, we can write

$$\kappa_\lambda(x) = \alpha_\lambda(x) + \beta_\lambda(x) \tag{5}$$

where $\alpha_\lambda(x)$ is the volume absorption coefficient and $\beta_\lambda(x)$ is the volume scattering coefficient. The extinction coefficient can also be divided into components representative of the attenuation properties of the medium. Thus,

$$\kappa_\lambda(x) = \kappa_{R\lambda}(x) + \kappa_{A\lambda}(x) \tag{6}$$

where $\kappa_{R\lambda}(x)$ is the extinction coefficient due to the gaseous component and $\kappa_{A\lambda}(x)$ is the extinction coefficient due to the aerosol component. Since we will assume in this report that we are dealing with a horizontally homogeneous atmosphere we shall consider the variability of the atmosphere parameters in the z (vertical) direction only.

The coefficients for absorption, scattering, and extinction can be expressed as

$$\alpha_\lambda(z) = N(z)\sigma_a(\lambda) \tag{7}$$

$$\beta_\lambda(z) = N(z)\sigma_s(\lambda) \tag{8}$$

$$\kappa_\lambda(z) = N(z)\sigma_t(\lambda) \tag{9}$$

where $N(z)$ is the number of independent centers of interaction and $\sigma_a(\lambda)$, $\sigma_s(\lambda)$, and $\sigma_t(\lambda)$ are the absorption, scattering, and total cross sections respectively. For a pure, aerosol-free atmosphere there is only the gaseous part of the attenuation to consider and the absorption cross section is calculated or measured for whatever spectral region is considered. The Rayleigh (gaseous) scattering cross section is given by

$$\sigma_s(\lambda) = \frac{8\pi^3(m(\lambda)^2-1)^2}{3\lambda^4 N^2}\left(\frac{6+3\rho}{6-7\rho}\right) \tag{10}$$

where ρ is the depolarization parameter ($\rho = 0.035$), N is the number of molecules per unit volume, and $m(\lambda)$ is the refractive index of air. The index $m(\lambda)$ is given by

$$m(\lambda) = 1.000064328 + \frac{0.02949810}{146 - 1/\lambda^2} + \frac{0.00025540}{41 - 1/\lambda^2} \tag{11}$$

for dry air at standard temperature and pressure of 15°C and 1013.250 mb. The wavelength λ in Eq. (11) has the units of micrometers. For any temperature t and pressure p other than the standard values t_s and p_s, the refractive index is given by

$$m(\lambda) = 1 + (m_s(\lambda)-1)\frac{t_s}{t}\frac{p}{p_s} \tag{12}$$

Hence, we can determine the Rayleigh cross section and the Rayleigh scattering coefficient for any altitude.

The corresponding cross sections for particulates involve much greater complications for several reasons: (1) uncertainty concerning the structure, (2) composition, (3) sizes, (4) and shape of the particles. If we make the assumption, however, that the particles can be represented by uniform, homogeneous spheres, then we can calculate the cross sections by using classical electromagnetic theory. These calculations were first performed by Lorenz[10] in 1890 and by Mie[11] in 1908 and the resulting formulation is known as Mie theory. The scattering, absorption, and total cross section for particles of radius r are given by the following:

$$\sigma_{s\lambda}(r) = \pi r^2 Q_s = \frac{2\pi r^2}{x^2} \sum_{\ell=1}^{\infty} (2\ell + 1)\left[|a_\ell|^2 + |b_\ell|^2\right] \tag{13}$$

$$\sigma_{a\lambda}(r) = \pi r^2 Q_a = \sigma_{t\lambda}(r) - \sigma_{s\lambda}(r) \tag{14}$$

$$\sigma_{t\lambda}(r) = \pi r^2 Q_t = \frac{2\pi r^2}{x^2} \sum_{\ell=1}^{\infty} (2\ell + 1) R_e(a_\ell + b_\ell) \tag{15}$$

where the parameters a_ℓ and b_ℓ are given in terms of Ricatti-Bessel functions, and the dimensionless parameter $x = 2\pi r/\lambda$. The factors Q_s, Q_a, and Q_t are referred to as the efficiency factors. As the particle size increases Q_s and Q_t approach the value of 2 whereas Q_a approaches zero. Hence, very large particles have cross sections which are twice their geometrical values. It is beyond the scope of this report to go into greater detail concerning the extensive subject of single-particle scattering theory. A full treatment of this work is given by Stratton [12], van de Hulst[13], and Kerker[14].

From Eq. (10) it is seen that the spectral dependence of a Rayleigh atmosphere is approximately λ^{-4}. For a hazy atmosphere the spectral dependence is a more slowly varying function of wavelength and is given by $\sim\lambda^{-1.3}$.

For aerosols with any size distribution n(r) the formulas for the absorption, scattering, and extinction coefficients are given by

$$\alpha_\lambda = \int_o^\infty n(r)\sigma_a(r)dr \tag{16}$$

$$\beta_\lambda = \int_o^\infty n(r)\sigma_s(r)dr \tag{17}$$

$$\kappa_\lambda = \int_o^\infty n(r)\sigma_t(r)dr \tag{18}$$

Another concept which is useful in radiative-transfer analysis, is the optical depth and optical thickness of the atmosphere. The optical depth $\tau_\lambda(h)$ at some altitude h in the atmosphere can be defined as

$$\tau_\lambda(h) = \int_h^\infty \kappa_\lambda(z)dz \ . \tag{19}$$

Thus, optical depth, a dimensionless quantity, represents the amount of material above altitude h. If we are at the bottom of the atmosphere, the optical thickness is then given by

$$\tau_{o\lambda} = \int_o^\infty \kappa_\lambda(z)dz \ . \tag{20}$$

For practical considerations, Koschmieder [15] developed a formula relating visual range at sea level to the volume extinction coefficient κ at the peak of the human eye response at a wavelength of 0.55μm. This relationship is depicted in Fig. 4.

Taking values of the molecular number density for the U.S. Standard Atmosphere and the Rayleigh cross section of Eq. (10) we have integrated the volume extinction coefficient over altitude to determine the optical thickness of the atmosphere [16]. This is illustrated in Fig. 5. Making use of Koschmieder's formula relating extinction coefficient and horizontal visual range and using results of measurements of light scattering in the

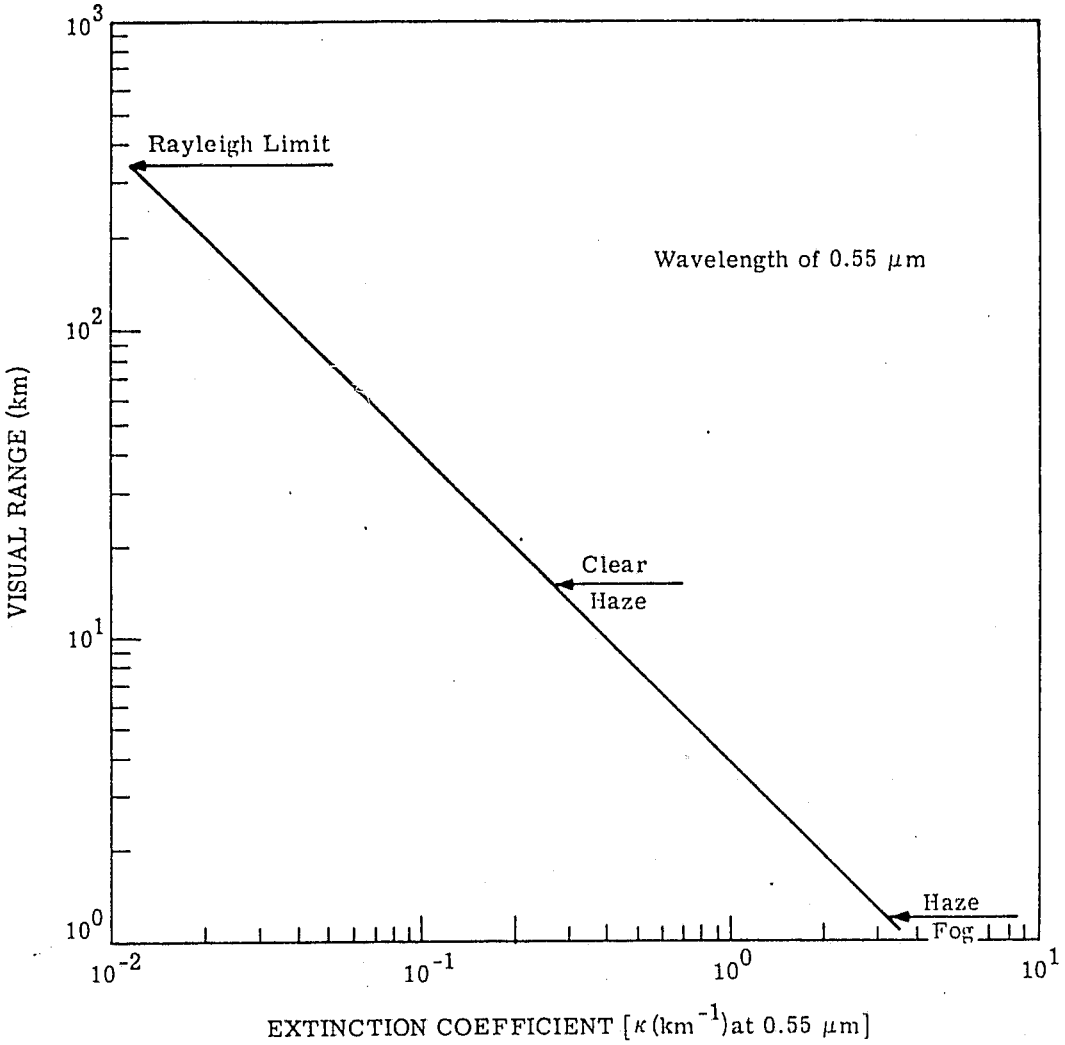

FIGURE 4. VARIATION OF VISUAL RANGE WITH EXTINCTION COEFFICIENT

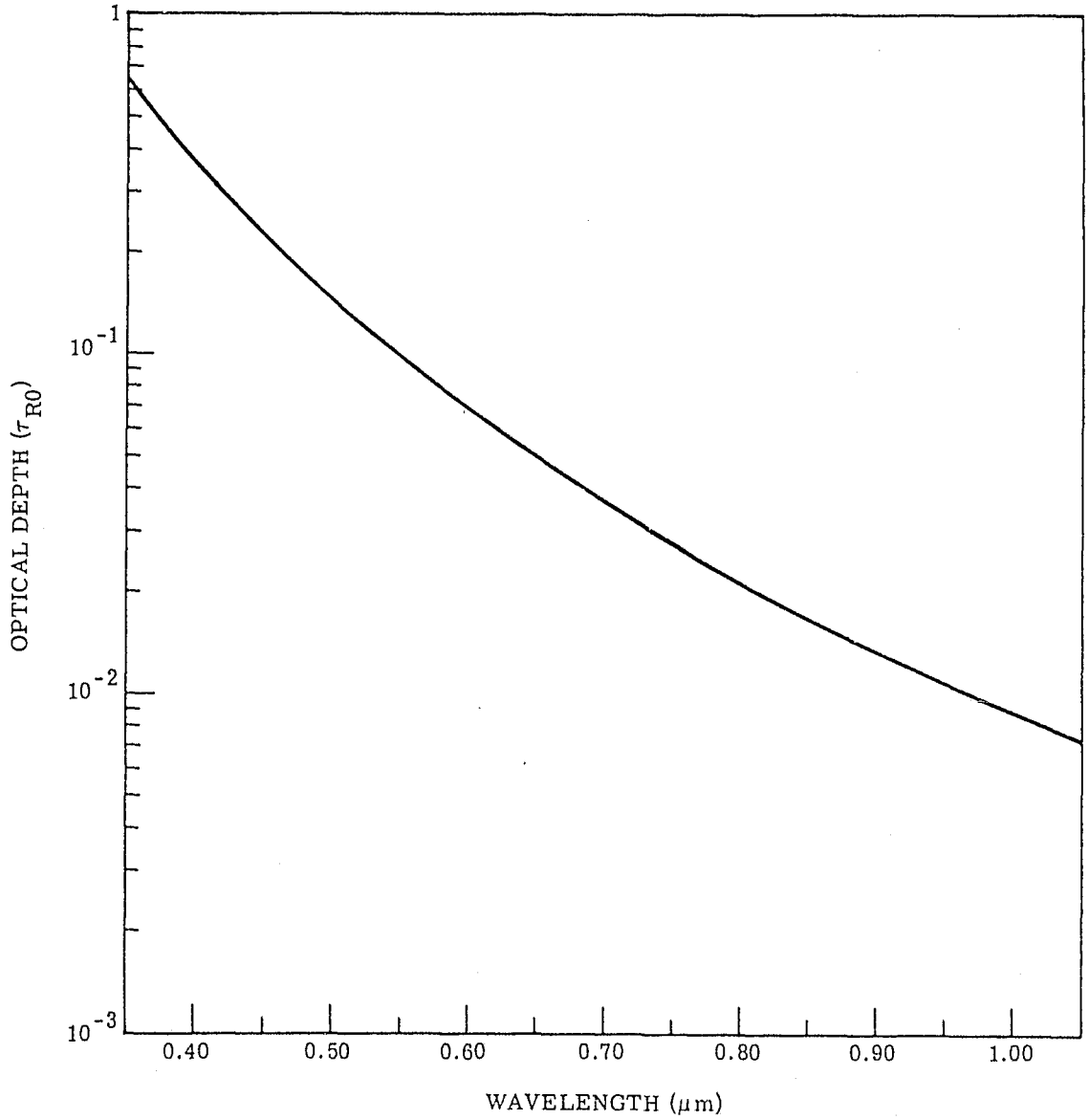

FIGURE 5. DEPENDENCE OF TOTAL RAYLEIGH OPTICAL DEPTH τ_{R0} ON WAVELENGTH FOR UNITED STATES STANDARD ATMOSPHERE.

atmosphere, Elterman [17] has formulated a model for hazy atmospheres. This model relates optical thickness, altitude, wavelength, and visual range. We have plotted his results in Fig. 6.

3.3 Climatology

If we assume radiative equilibrium for the Sun-Earth-Atmosphere system the equivalent "brightness" temperature T_s can be defined as follows:

$$T_s = \left[\frac{(1-A)E_o}{4\sigma}\right]^{1/4} \tag{21}$$

where E_o is the extra-terrestrial irradiance (flux) incident at the top of the atmosphere, σ is the Stefan-Boltzmann constant, and A is the albedo of the Earth-atmosphere system. Using a value of 1353 Wm^{-2} for the solar flux we can calculate the temperature. This is illustrated in Fig. 7. It should be noted that the largest change in temperature occurs when the albedo is quite high ($A \gtrsim 0.9$). Estimates of the planetary albedo usually range from 0.30 to 0.40. Thus, a more detailed plot of the temperature for a realistic albedo range is presented in Fig. 8. If we have a planetary albedo of about 0.33 then according to Eq. (21) or Fig. 8 we have a temperature of 251.5°K, a value close to the satellite observations of Raschke and Bandeen [18]. This temperature is, however, much lower than the mean surface temperature of Earth which is about 286°K. The reason is due to the effect of the absorption of outgoing infrared radiation, primarily by the gases, carbon dioxide and water vapor and by clouds which re-emit radiation downward to keep the surface temperature high. This is usually referred to as the "Greenhouse" effect. Thus, the Earth's temperature is actually a function of the albedo of the Earth-atmosphere system, the incoming solar flux, and the composition of the atmosphere. The Earth's surface and hence the surface albedo has undergone changes over the years. The building of roads and highways alone has taken about one percent of the land area in the United States. Large-scale land cultivation and irrigation has also changed the surface albedo. In addition, a decrease in the forest areas

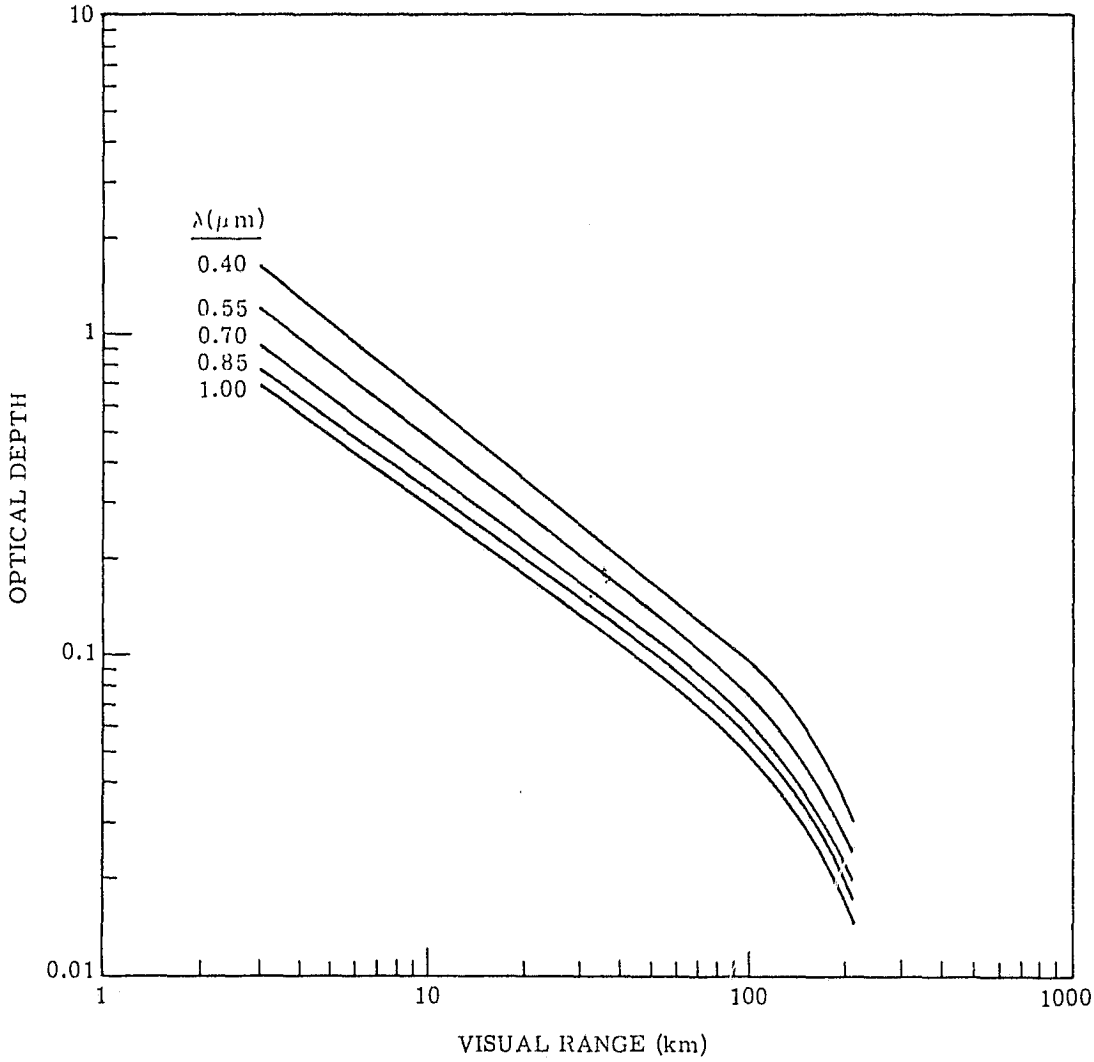

FIGURE 6. AEROSOL OPTICAL DEPTH τ_A VERSUS VISUAL RANGE V. Parameter is spectral wavelength, λ.

FIGURE 7
HYPOTHETICAL EARTH
TEMPERATURE AS A
FUNCTION OF ALBEDO

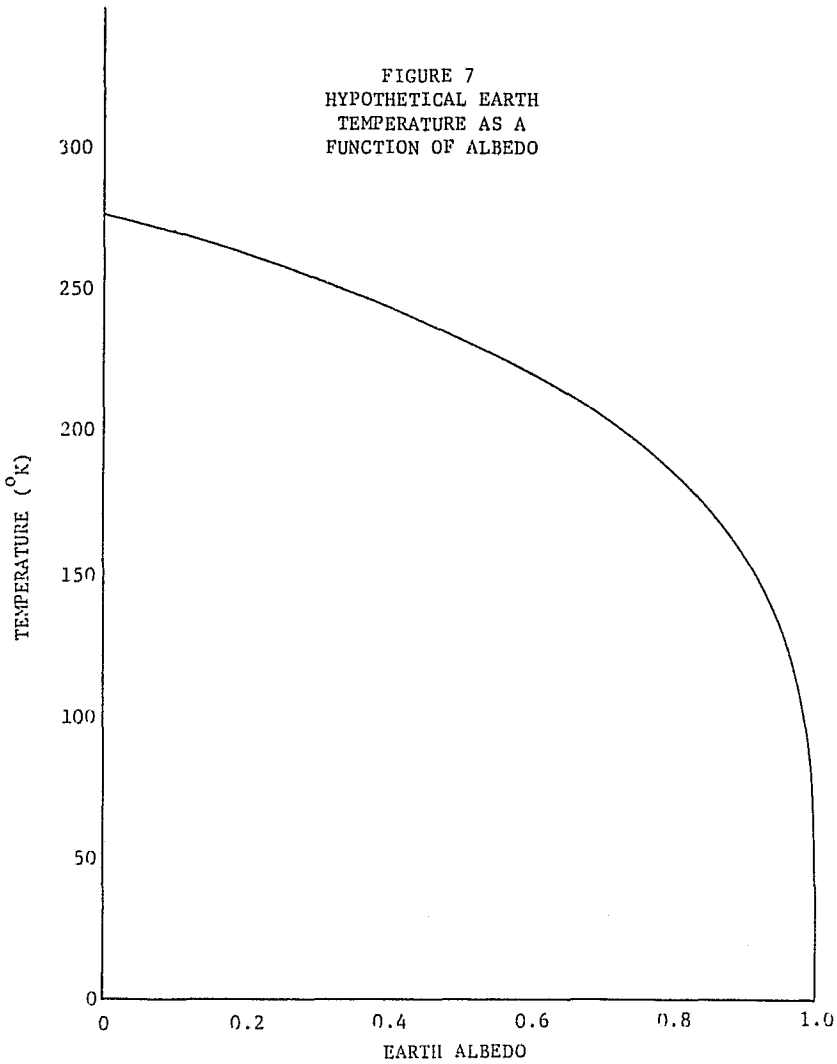

FIGURE 8
HYPOTHETICAL EARTH TEMPERATURE
AS A FUNCTION OF ALBEDO IN
REGION OF REALISTIC ALBEDO

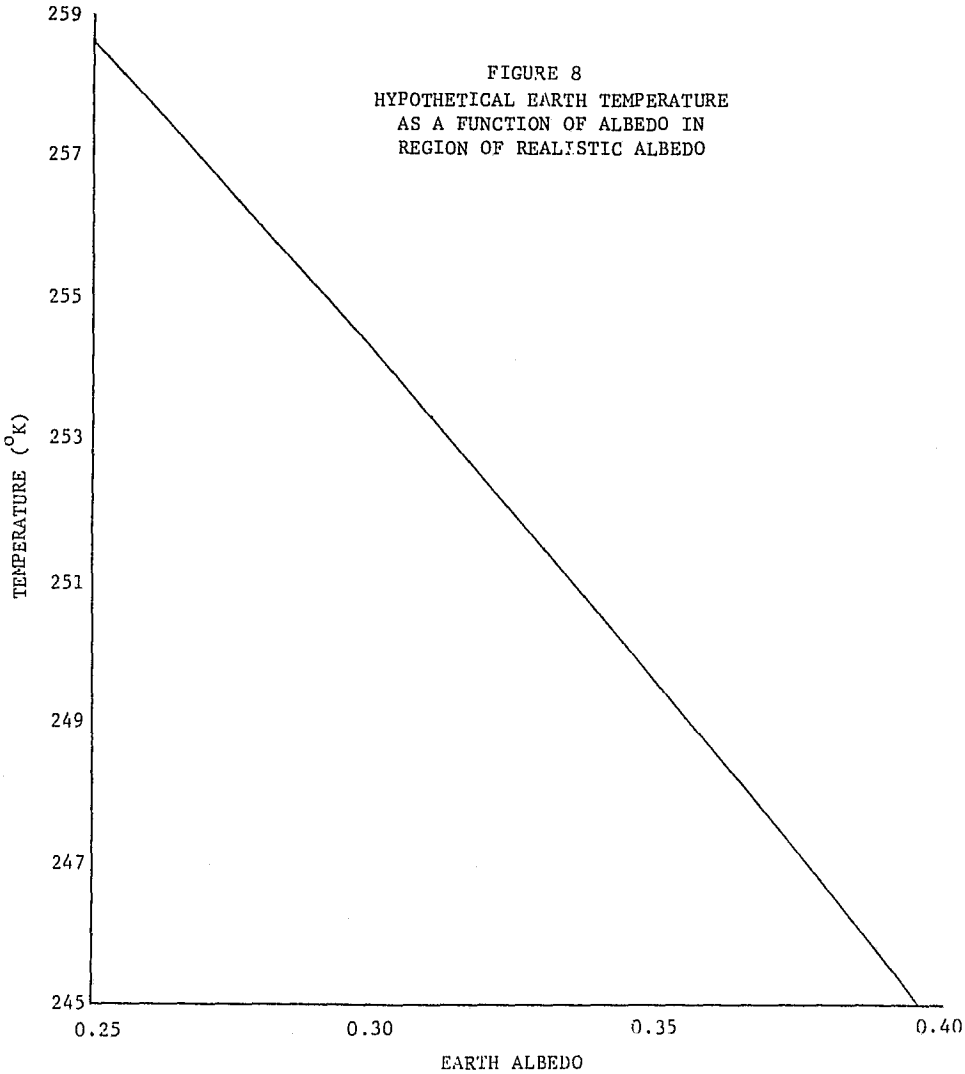

could produce serious climatic effects since the amount of carbon dioxide in the atmosphere is dependent upon the biomass.

The role of particulates in determining the temperature of the Earth is now being investigated. In fact, the increase in the atmospheric particulate load could reflect solar radiation to such an extent that the mean temperature of Earth will decrease by 3.5°K over a period of several years. Rasool and Schneider[19] have performed calculations using a two-stream model for the transfer of radiation through the atmosphere. The predicted decrease in temperature as a function of atmospheric optical thickness is illustrated in Fig. 9. Other recent calculations[20] also indicate that a net heating effect could result from an increase of the particulates and also from an increase in the chlorofluorocarbons[21] or Freons. Clearly, the problem is far from being solved; more reliable data are needed on the question of the increase of those gaseous components which enhance the Greenhouse effect and, also better atmospheric models should be used in the analysis of temperature changes.

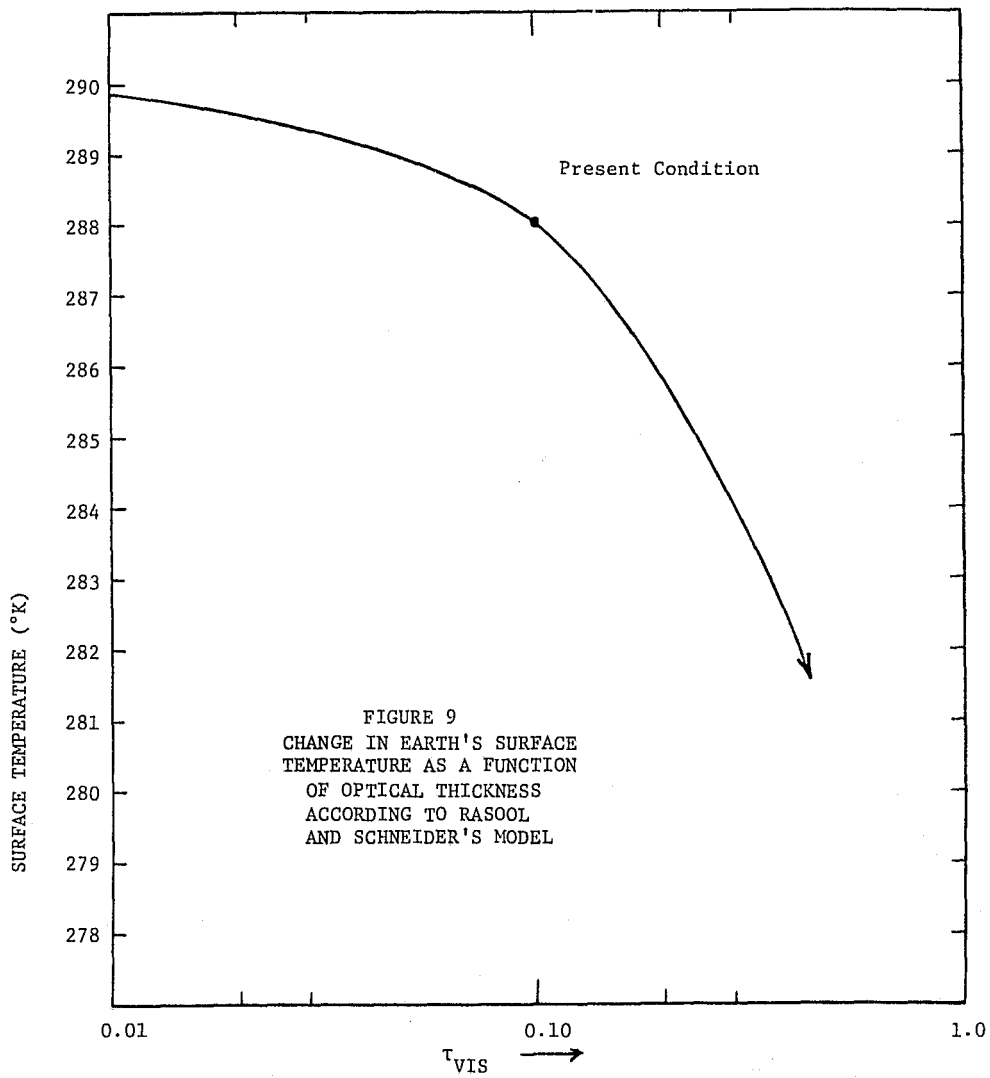

FIGURE 9
CHANGE IN EARTH'S SURFACE TEMPERATURE AS A FUNCTION OF OPTICAL THICKNESS ACCORDING TO RASOOL AND SCHNEIDER'S MODEL

4

THE ATMOSPHERIC MODEL

In this chapter we shall consider the basic atmospheric-radiative-transfer model which was used for the analysis of SKYLAB data and for aerosol albedo studies.

4.1 Radiometry

In this section we shall define the basic radiometric terms which are used in radiative-transfer theory.

4.1.1 Radiance

The radiance L is defined as the radiant power that leaves a surface per unit solid angle and unit projected area of that surface. This can be expressed mathematically as

$$L \equiv \frac{\partial^2 P}{\partial A \, \partial \Omega \cos \theta} \tag{22}$$

where P is the radiant power, A is the area, Ω is the solid angle, and θ is the angle between the direction of the outgoing radiation and the surface normal vector. Usually we shall be concerned with the spectral radiance; the units will be mW/cm^2-sr-μm. It is well known that the apparent brightness of an object is invariant with distance. The total flux decreases as one gets farther from an illuminated source but the amount of power density per unit solid angle is constant. Thus the radiance-invariance law which for two media with different indices of refraction can be expressed as

$$\frac{L_1}{n_1^2} = \frac{L_2}{n_2^2} \tag{23}$$

4.1.2 Irradiance

The irradiance E is defined as the radiant power incident upon a surface per unit area, i.e.

$$E \equiv \frac{\partial P}{\partial A} \tag{24}$$

a quantity which does depend upon distance. We shall use the units of mW/cm^2-μm. for spectral irradiance. For a more complete definition of these radiometric terms and their conceptual foundations the work of Preisendorfer [23] is recommended.

From Eqs (22) and (23) we see that the irradiance can be found if the radiance is known over a hemisphere, i.e.

$$E = \int_{\Omega} L \cos\theta \, d\Omega \tag{25}$$

where Ω is one hemisphere or 2π steradians.

4.1.3 Transmittance

The transmittance of a beam of radiation propagating through the atmosphere lies somewhere between zero and unity. For zero transmittance no direct radiation passes through the medium and for a value of one all the radiation passes through undiminished in intensity. We shall neglect gaseous absorption in this report because we are primarily interested in the scattering of radiation by gases and aerosols.

If an infinitesimal, narrow beam of monochromatic radiation propagates through a medium the intensity at distance x from the source is

$$I_\lambda(x) = I_\lambda(o) T_\lambda(x) \tag{26}$$

where $I_\lambda(o)$ is the source intensity at wavelength λ and $T_\lambda(x)$ is the spectral transmittance at distance x. If the loss of radiation from the beam is total, i.e., complete absorption and/or scattering out of the beam then the fractional change in intensity is given by the following:

$$\frac{\Delta I_\lambda(x)}{I_\lambda(x)} = - \kappa_\lambda(x)\, \Delta x \tag{27}$$

where $\kappa_\lambda(x)$ is the probability per unit length for a net loss of radiation from the beam and Δx is the distance over which the fractional change occurs. As the length Δx approaches zero we have

$$\frac{dI_\lambda(x)}{dx} = - \kappa_\lambda(x)\, I_\lambda(x) \tag{28}$$

$$I_\lambda(x) = I_\lambda(o)\, e^{-\int_o^x \kappa_\lambda(x')dx'} \tag{29}$$

Thus, we see that the spectral transmittance $T_\lambda(x)$ is given by

$$T_\lambda(x) = e^{-\int_o^x \kappa_\lambda(x')dx'} \tag{30}$$

Hence, one of the problems is to determine the probability per unit length $\kappa_\lambda(x)$. It can be determined experimentally or theoretically by applying the Mie scattering theory for particles. The quantity in the exponential in Eq. (30) is called the optical depth of the medium. For a vertical distribution through Earth's atmosphere the spectral transmittance would be given by

$$T_\lambda = e^{-\int_o^\infty \kappa_\lambda(z')dz'} \tag{31}$$

The transmittance versus optical depth is depicted in Fig. 10.

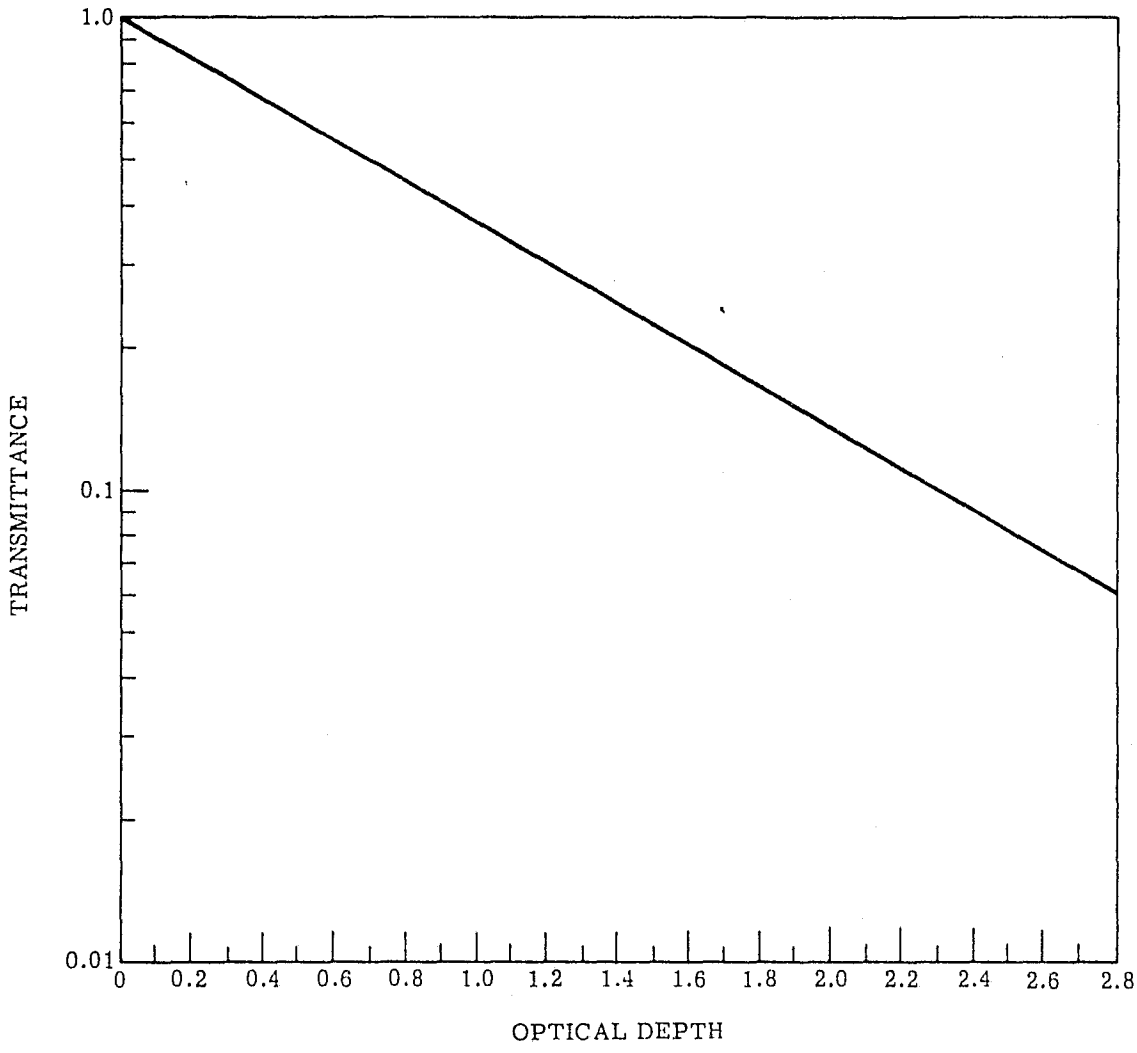

FIGURE 10. TRANSMITTANCE T VERSUS OPTICAL DEPTH τ.

4.2 Reflectance

4.2.1 Non-Lambertian

In general, radiation incident on a surface may be reflected at any angle. If the incident radiation is represented by the zenith angle $\theta'(= \cos^{-1}\mu')$ and an azimuthal angle ϕ' and the outgoing reflected radiation is represented by corresponding angles θ and ϕ, then the bi-directional reflectance can be defined by the relation

$$L(\mu,\phi) = \int_0^{2\pi} \int_0^1 \mu' \rho'(\mu,\phi,\mu',\phi') \, L\,(-\mu',\phi') d\mu' d\phi' \tag{32}$$

Hence, the reflectance properties of a surface are in general represented by four independent angles. For specular surfaces there is a known relationship connecting the incoming and outgoing radiation, i.e.

$$\mu = \mu' \; ; \; \phi = \phi' + \pi \tag{33}$$

or

$$\rho'_{spec}\,(\mu,\phi,\mu',\phi') = \frac{1}{\mu'}\,\delta(\mu'-\mu)\delta(\phi'-\phi-\pi) \tag{34}$$

Thus, Eq. (32) becomes

$$L(\mu,\phi) = L(-\mu,\, \phi + \pi) \tag{35}$$

Many surfaces have been studied to determine their bidirectional reflectance [23], a large collection of which exhibit some specular characteristics.

4.2.2 Lambertian

If the surface has no dependence on angles then we say that the surface is Lambertian or perfectly diffuse. In this case, Eq. (32) becomes

$$L(\mu,\phi) = \rho' \, E \tag{36}$$

where E is the irradiance on the surface. If we now integrate Eq. (36) over the outgoing angles, θ and ϕ, we have

$$\int_0^{2\pi}\int_0^1 \mu\, L(\mu,\phi)\, d\mu d\phi = \int_0^{2\pi}\int_0^1 \rho'\, \mu\, E\, d\mu d\phi \tag{37}$$

or

$$M = \pi\rho' E \tag{38}$$

where M is defined as the radiant exitance. By definition the ratio of exitance to irradiance is the albedo of the surface. Designating the albedo or perfectly diffuse reflectance by ρ we have

$$M = \rho E \tag{39}$$

so that Eq. (32) becomes

$$L(\mu,\phi) = \frac{\rho}{\pi} E \tag{40}$$

for a Lambertian surface. Although such a surface is unrealistic, the approximation is used to simplify analysis. Also, for many natural materials such as soil and plants the approximation is probably not too bad for the visible part of the spectrum. A compilation of reflectance has been produced by Leeman et al.[24] for over 3800 materials.

4.3 Radiative-Transfer Theory

It is beyond the scope of this report to go into the details of radiative-transfer theory. Instead, we shall consider various solutions of the radiative-transfer equation in order to apply the theory to the investigation of the albedo of the Earth-atmosphere system. A more complete

treatment of radiative-transfer theory is given by Anding et al.[25], Malila et al.[26], Turner and Spencer [27], Horvath et al.[16], Turner [28,29,30], Turner et al.[31], and LaRocca and Turner[32].

4.3.1 The Radiative-Transfer Equation

Since we are concerned with the steady-state condition of the transfer of energy in the atmosphere, we can use the time-independent radiative-transfer equation

$$\hat{\Omega} \cdot \nabla L(\vec{r},\hat{\Omega}) + \kappa(\vec{r})L(\vec{r},\hat{\Omega}) - \frac{\beta(\vec{r})}{4\pi}\int_{\hat{\Omega}'} p(\vec{r},\hat{\Omega}\cdot\hat{\Omega}')L(\vec{r},\hat{\Omega}')d\hat{\Omega}' = Q(\vec{r},\hat{\Omega}) \qquad (41)$$

in which $\hat{\Omega}'$ is the incoming radiance vector, and $\hat{\Omega}$ is the outgoing radiance vector. Since we are not considering polarization, the spectral radiance $L(\vec{r},\hat{\Omega})$ is a scalar. The quantity $\kappa(\vec{r})$ is the volume extinction coefficient, $\beta(\vec{r})$ is the volume scattering coefficient, and $Q(\vec{r},\hat{\Omega})$ is the source term. The integral term represents the contribution of radiation as a result of multiple scattering at point $\vec{r}$ in the medium according to a particular angular distribution disignated by the single-scattering phase function $p(\vec{r},\hat{\Omega}\cdot\hat{\Omega}')$. The three-dimensional radiative-transfer equation does have an exact solution for certain cases [30], [33], but for our purposes we shall consider a one-dimensional equation in which the only spatial variability occurs in the vertical (z) direction. For solar radiation entering the top of Earth's atmosphere with a zenith angle $\theta_o (= \cos^{-1}\mu_o)$ and an azimuthal ϕ_o, the one-dimensional radiative-transfer equation is

$$\mu \frac{dL}{d\tau} = L(\tau,\mu,\phi) - \frac{\omega_o(\tau)}{4\pi}\int_0^{2\pi}\int_{-1}^{1} p(\tau,\mu,\phi,\mu',\phi')\, L\,(\tau,\mu',\phi')d\mu'd\phi'$$

$$- \frac{\omega_o(\tau)}{4\pi}\, E_s(\tau)p(\tau;\mu,\phi,-\mu_o,\phi_o) \qquad (42)$$

in which $\omega_o(\tau)$ is called the single-scattering albedo and $E_s(\tau)$ is the solar irradiance at optical depth τ. We are assuming no thermal emission.

4.3.2 Formal Solutions

If we assume a vertically homogeneous plane-parallel atmosphere, i.e. one in which neither the single-scattering albedo, $\omega_o(\tau)$ nor the single-scattering phase function, $p(\tau;\mu,\phi,\mu',\phi')$ depend upon optical depth, then the formal solutions of Eq. (42) are the following:

$$L(\tau,\mu,\phi) = L(\tau_o,\mu,\phi)e^{-(\tau_o-\tau)/\mu} + \frac{\omega_o}{4\pi\mu}\int_0^{2\pi}\int_{-1}^{1} p(\mu,\phi,\mu',\phi')\int_\tau^{\tau_o} e^{-(\tau'-\tau)/\mu}L(\tau',\mu',\phi')d\tau'd\mu'd\phi' + \frac{\omega_o\mu_o E_o p(\mu,\phi,-\mu_o,\phi_o)}{4\pi(\mu+\mu_o)}\left[e^{-\tau/\mu_o} - e^{-\tau_o/\mu_o}e^{-(\tau_o-\tau)/\mu}\right] \quad (43)$$

for the upwelling radiation, and

$$L(\tau,-\mu,\phi) = L(0,-\mu,\phi)e^{-\tau/\mu} + \frac{\omega_o}{4\pi\mu}\int_0^{2}\int_{-1}^{1} p(-\mu,\phi,\mu',\phi')\int_0^{\tau} e^{-(\tau-\tau')/\mu}L(\tau',\mu',\phi')d\tau'd\mu'd\phi' + \frac{\omega_o\mu_o E_o p(-\mu,\phi,-\mu_o,\phi_o)}{4\pi(\mu-\mu_o)}\left[e^{-\tau/\mu} - e^{-\tau/\mu_o}\right] \quad ; \mu \neq \mu_o \quad (44)$$

for the downwelling radiation.

The boundary conditions are

$$L(0,-\mu,\phi) = 0 \tag{45}$$

i.e. it is assumed that there is no diffuse radiation entering the top of the atmosphere, and

$$L(\tau_o,\mu,\phi) = \int_0^{2\pi}\int_0^1 \mu' p(\mu,\phi,\mu',\phi') \left[L_{SOL}(\tau_o,-\mu',\phi') + L_{SKY}(\tau_o,-\mu',\phi')\right] d\mu' d\phi' \tag{46}$$

Hence, Eqs. (43) and (44) together with the boundary conditions, Eqs. (45) and (46) should allow us to determine the complete radiation field in the atmosphere. It is interesting to note that Eq. (43) can be written in the compact form

$$L = L_o T + L_p \tag{47}$$

where L_o is the surface (target) radiance, T is the transmittance between the surface (target) and the sensor, and L_p is the so-called path radiance, i.e. that radiance which arises from singly or multiply scattered radiation into the instantaneous field of view. Equation (47) can also be thought of as the remote sensing equation. Likewise, if we are at the bottom of the atmosphere ($\tau=\tau_o$) then the sky radiance is given by Eq. (44) with $\tau=\tau_o$.

4.3.3 Approximate Solutions

The radiative-transfer equation, either in its differential form, Eq. (42) or its integral forms, Eqs. (43),(44), is quite difficult to solve. Exact solutions do exist for special cases [34,35], but for the

general cases of a realistic atmosphere with an aerosol distribution elaborate mathematical techniques must usually be employed to find a solution. One of the main reasons why the equation is so difficult to solve is that the scattering of radiation by an aerosol particle is highly anisotropic; the scattering is predominantly in the forward direction. This is illustrated in Fig. 11. Mathematically, the highly anisotropic phase function can be represented by a series of Legendre polynominals but the number of terms required to represent the function adequately is usually quite large. This means that various analytic solutions are complicated or require a considerable expenditure of computer time.

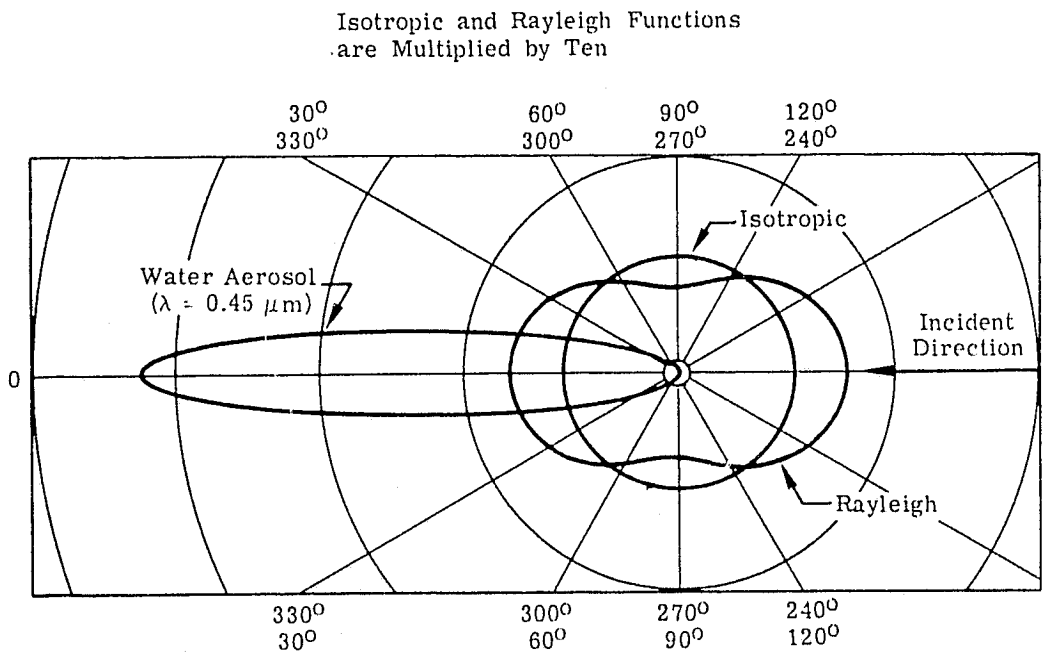

FIGURE 11. ANGULAR DEPENDENCE OF SINGLE-SCATTERING PHASE FUNCTIONS IN ANY AZIMUTHAL PLANE.

For these reasons, we shall consider a simpler solution of the radiative-transfer equation. For a first approximation let us represent the single-scattering phase function by two-streams, one in the forward direction and one in the backward direction. Thus,

$$p(\mu,\phi,\mu',\phi') = 4\pi\eta\delta(\mu-\mu')\delta(\phi-\phi') + 4\pi(1-\eta)\delta(\mu+\mu')\delta(\pi+\phi-\phi') \quad (48)$$

where η represents the fraction of radiation which is scattered into the forward hemisphere. For Rayleigh scattering $\eta = 0.5$, whereas for a hazy atmosphere $\eta \cong 0.96$. If we also represent the radiance by the same set of functions, i.e.

$$L(\tau,\mu,\phi) = \frac{1}{\mu_o}\left[E_+'(\tau)\delta(\mu-\mu_o)\delta(\pi+\phi_o-\phi) + E_-'(\tau)\delta(\mu+\mu_o)\delta(\phi-\phi_o)\right] \quad (49)$$

where $E_+'(\tau)$ and $E_-'(\tau)$ are the upward and downward diffuse fluxes for an atmosphere bounded by a black surface. Proceeding in a similar manner for non-black surfaces we can then insert expressions (48) and (49) into Eq. (42) in order to solve for the fluxes in the realistic atmosphere. The solutions are too lengthy to present here; they are given in Appendix I. These solutions will be used in the analysis of the SKYLAB data.

Using the flux equations along with an expression similar to that of Eq. (49) then allows us to calculate the path and sky radiances. These results are more complicated than those for the fluxes and they are given in Appendix II.

The accuracy of this model can be tested by comparing the results of the model calculations with other mathematically exact calculations and with experimental data. An example of a comparison with Chandrasekhar's exact calculations is illustrated in Fig 12. A comparison with experimental values of sky radiance are depicted in Fig. 13. In either case, the agreement is very good considering the fact that the model was not expected to conform to atmospheres with such a small aerosol content.

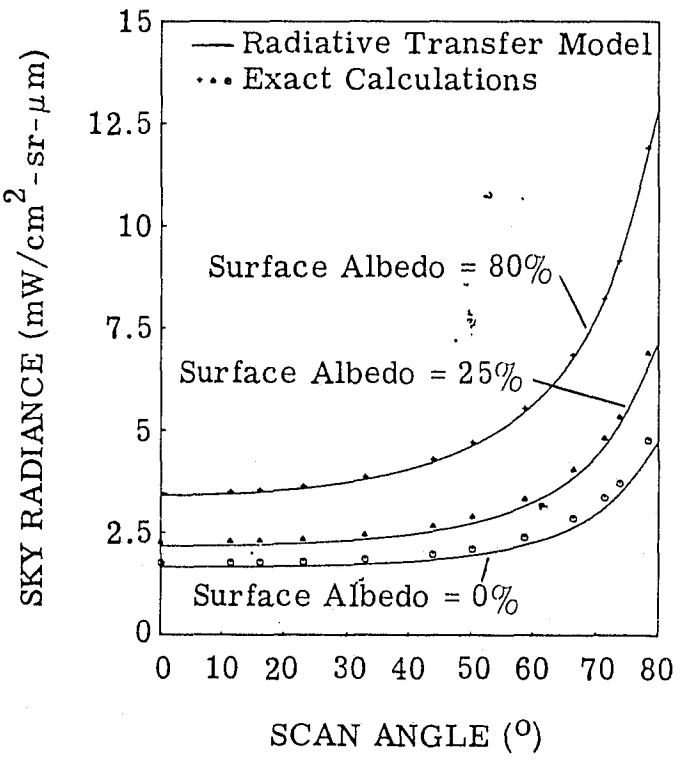

FIGURE 12. DEPENDENCE OF SKY RADIANCE ON SCAN ANGLE (PERPENDICULAR TO SOLAR PLANE) FOR A RAYLEIGH ATMOSPHERE. Wavelength = 0.546μm; solar zenith angle = 36.9°.

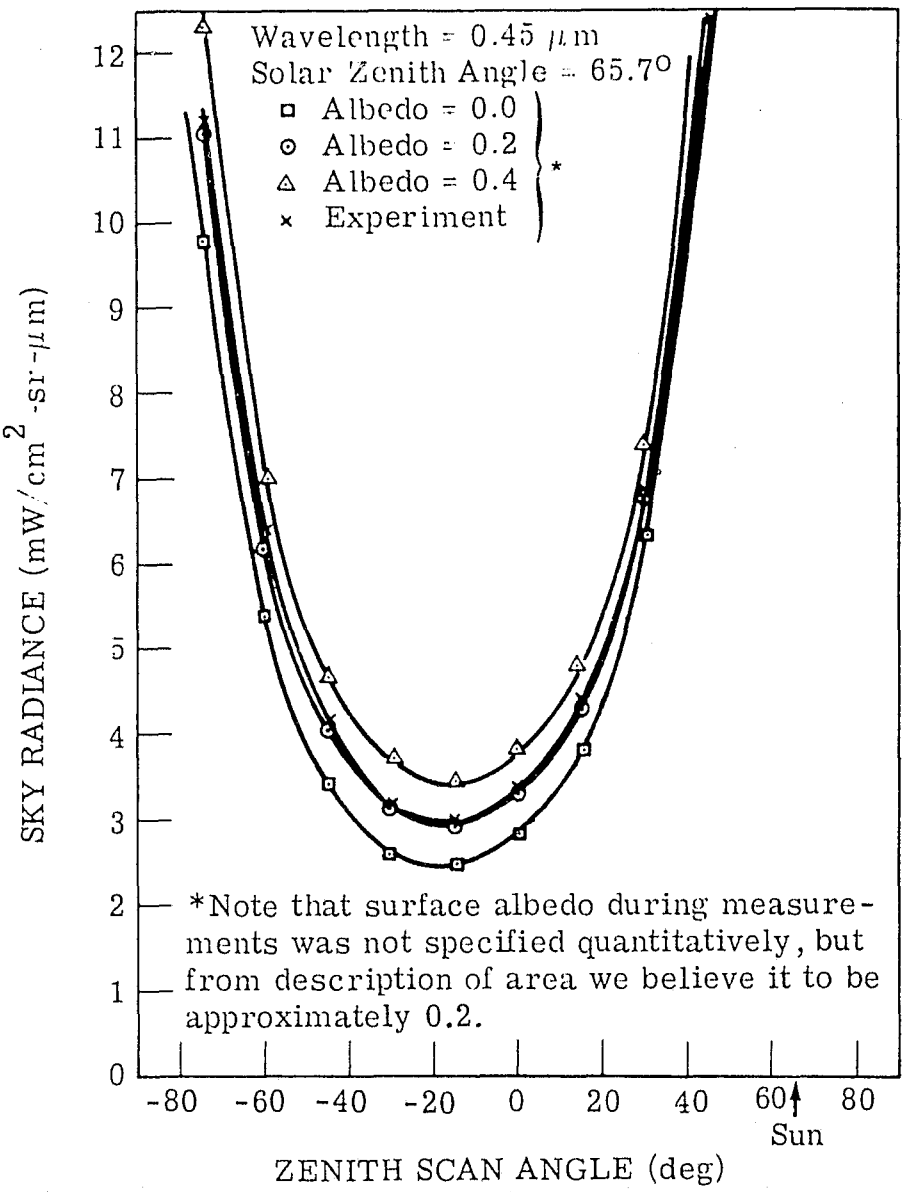

FIGURE 13. DEPENDENCE OF SKY RADIANCE ON ZENITH ANGLE (IN SOLAR PLANE) FOR CLEAR SKY CONDITIONS. Wavelength = 0.45μm; solar angle = 65.7°.

5

Albedo Calculations

In this chapter we shall calculate the albedo of the Earth-Atmosphere system using the radiative-transfer model and also develop mathematical relationships for energy conservation in realistic atmospheres.

5.1 Albedo

Albedo means the ratio of output power of a system to the input power and must therefore range in value from zero to one. In this report we consider three albedos and it is important that we define them carefully so that no confusion occurs. First, the single-scattering albedo, ω_o is the ratio of the volume scattering coefficient to the volume extinction coefficient and is a fundamental property of the medium at a given point. It can vary throughout the medium. Second, the surface albedo, ρ is the ratio of reflected power to incident power independent of an atmosphere. Third, we shall consider the total or planetary albedo, A of the Earth-Atmosphere system. The main object of the present investigation is to understand the effect which aerosols have on the albedo A.

The satellite determination of the albedo or the radiant exitance of a planet is not an easy task. By definition, the albedo concept involves the total power integrated over a hemisphere and a satellite measurement can only be done at selected small areas over a planetary surface. Essentially, what is measured is the total spectral radiance. In this case, the radiance of an atmosphere increases with increasing turbidity if the surface albedo is low, whereas the radiance will decrease if the surface albedo is high. This effect is illustrated in Fig. 14 in which the various atmospheric states are designated by the total transmittance.

The total flux incident upon a plane-parallel atmosphere is $\mu_o E_o$ where μ_o is the cosine of the solar zenith angle and E_o is the extra-terrestrial solar flux at the top of the atmosphere on a plane perpendicular to the sun. The radiant exitance is $E_+(o)$, the power density lost through the surface is $(1-\rho)\tilde{E}_-(\tau_o)$, and the power density lost by absorption

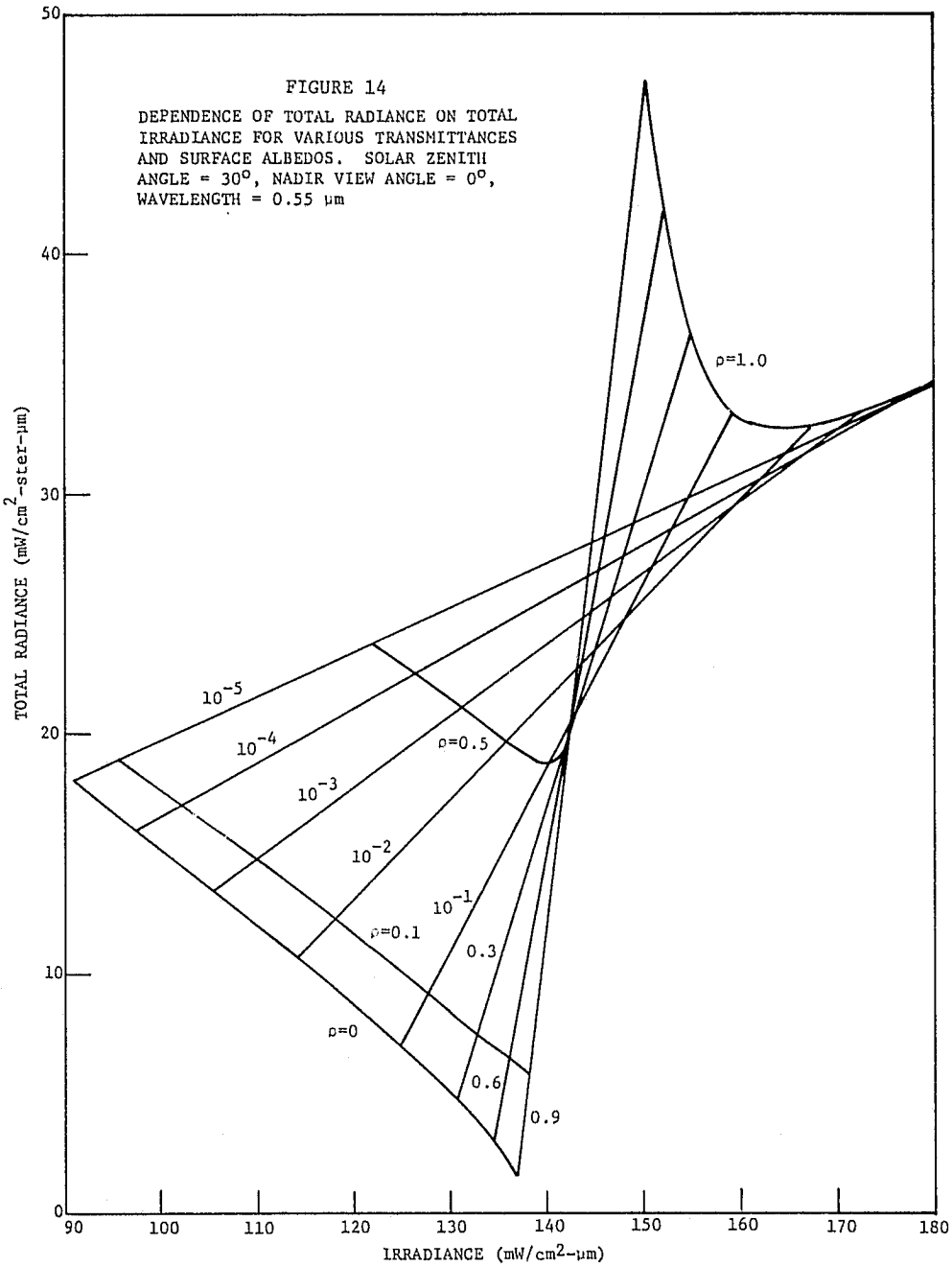

FIGURE 14

DEPENDENCE OF TOTAL RADIANCE ON TOTAL IRRADIANCE FOR VARIOUS TRANSMITTANCES AND SURFACE ALBEDOS. SOLAR ZENITH ANGLE = 30°, NADIR VIEW ANGLE = 0°, WAVELENGTH = 0.55 μm

in the atmosphere is $(1-\omega_o)E_\ell$. In order that energy be conserved we must have

$$\mu_o E_o = E_+(o) + (1-\rho)\tilde{E}_-(\tau_o) + (1-\omega_o)E_\ell \tag{50}$$

The albedo of the total Earth-Atmosphere system is then defined as

$$A \equiv E_+(o)/\mu_o E_o \tag{51}$$

or

$$A = 1 - \frac{(1-\rho)\tilde{E}_-(\tau_o)}{\mu_o E_o} - (1-\omega_o)\frac{E_\ell}{\mu_o E_o} \tag{52}$$

It is interesting to consider special cases of Eq. (52). If the atmosphere absorbs no radiation, i.e. $\omega_o = 1$ then, using the specific relations for fluxes given in Appendix I we have for a pure scattering atmosphere,

$$A = \frac{\mu_o\rho + (1-\eta)\tau_o\left[1 + 2(1-\eta)(1-\rho)\tau_o\right]}{\left[\mu_o + (1-\eta)\tau_o\right]\left[1 + 2(1-\eta)(1-\rho)\tau_o\right]} \tag{53}$$

and, as the atmosphere becomes optically very thin, i.e., as $\tau_o \to 0$ we see from Eq. (53) that $A \to \rho$.

Another interesting case is when the atmosphere becomes optically very thick, i.e. as $\tau_o \to \infty$. Here we have

$$A = \frac{(1-\eta)\omega_o}{1-\eta\omega_o + \sqrt{(1-\omega_o)(1+\omega_o - 2\eta\omega_o)}} \tag{54}$$

If, in addition, $\omega_o = 1$, we see that A = 1 as it should be. Such an atmosphere behaves as a perfect reflector. On the other hand, if $\omega_o = 0$ for this case we see that A = 0, a perfect absorber. A very simple relationship holds if we have a Rayleigh or an isotropic scattering law, i.e. $\eta = 1/2$. In this case

$$A = \frac{\omega_o}{2 - \omega_o + 2\sqrt{1-\omega_o}} \tag{55}$$

Some of these relationships can be illustrated as in Fig. 15. We have calculated the total albedo as a function of atmospheric optical thickness and surface albedo for a pure scattering atmosphere. The reason for the minimum is that the atmosphere was gradually changed from a Rayleigh atmosphere with $\eta = 1/2$ to an atmosphere with a greater aerosol contribution in which $\eta > 1/2$.

5.2 Energy Conservation Relations

Equation (52) can be rewritten as follows:

$$A + (1-\rho)\tilde{F}_- + (1-\omega_o)F_\ell = 1 \tag{56}$$

This conservation relation can be illustrated graphically by considering each component to be the length of a perpendicular in an equilateral triangle of unit altitude. Such a relationship is illustrated in Fig. 16. Any planetary state can be represented by a point located somewhere within the triangle. A planetary system with low surface albedos and very little absorption will have points in the lower right corner of the diagram. A system with low surface albedo and strong absorption will have points along the left side of the diagram and systems with high

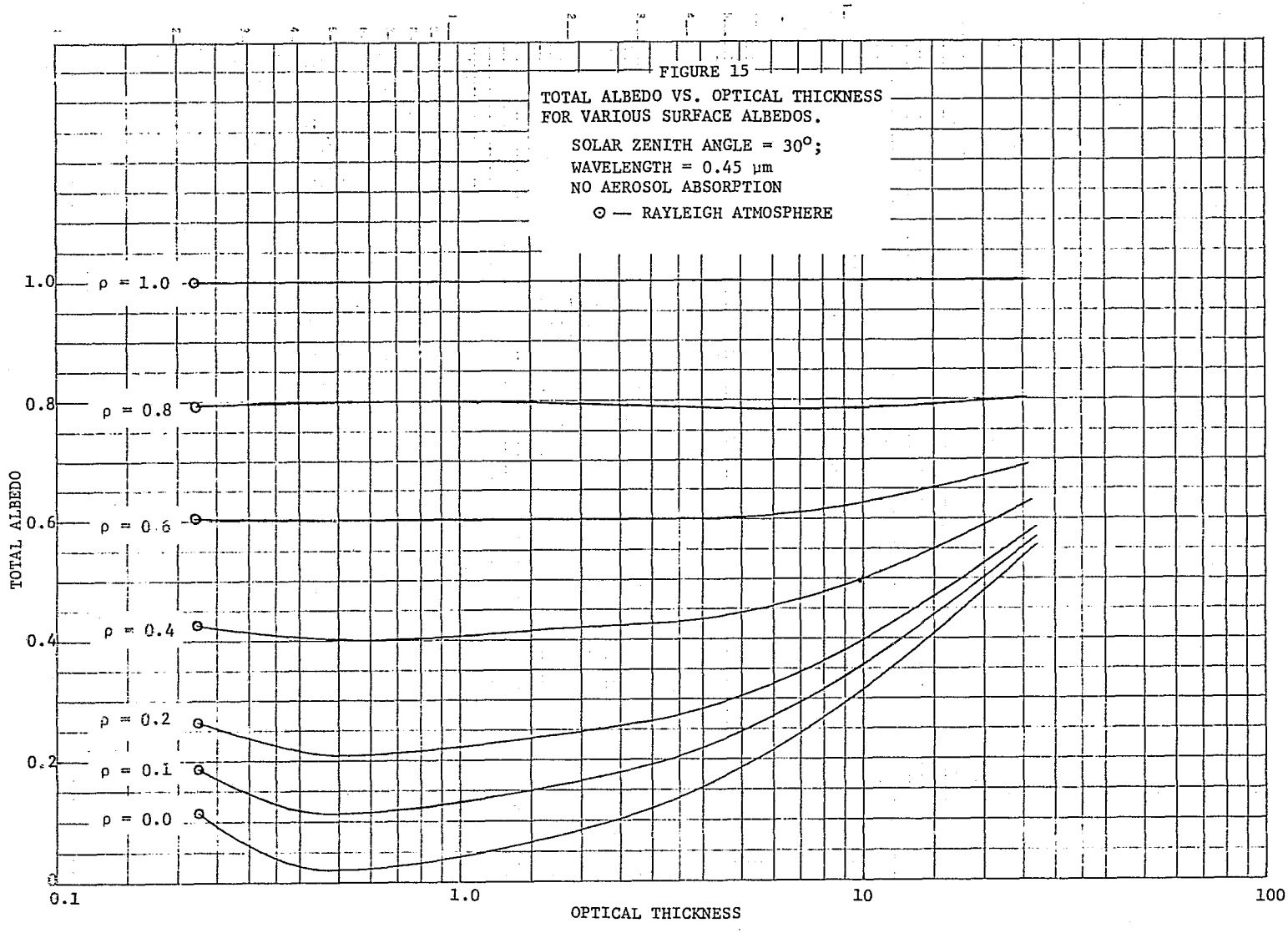

FIGURE 15

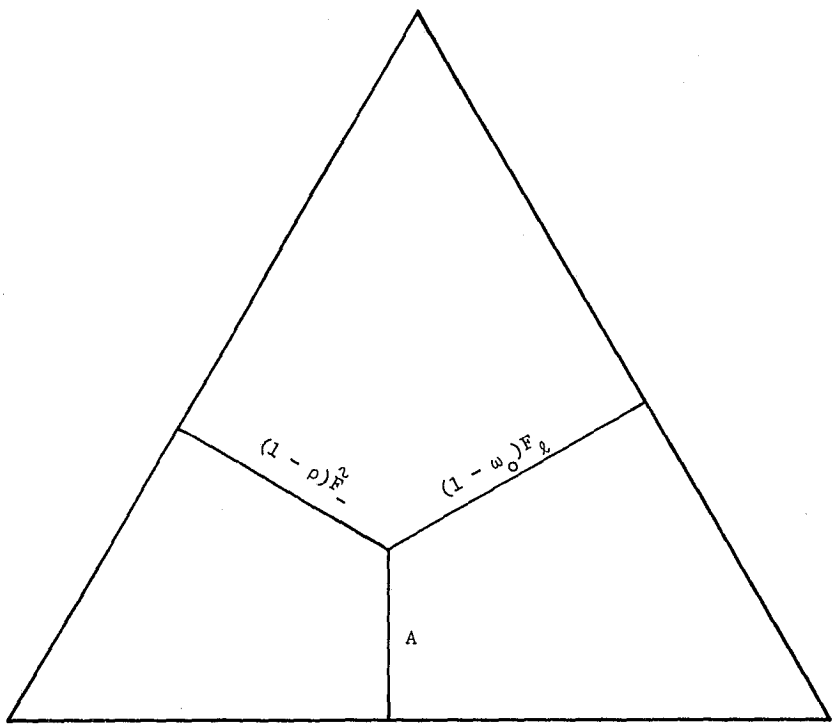

FIGURE 16
ENERGY CONSERVATION RELATION FOR
REALISTIC PLANETARY ATMOSPHERES

A ∿ Total Albedo

$(1-\rho)\tilde{F}_-$ ∿ Surface Flux Loss

$(1-\omega_o)F_\ell$ ∿ Atmospheric Flux Loss

surface albedos and very little absorption will have points in the upper corner of the diagram. Hence, if a series of measurements are taken the energy loss of an atmosphere can be estimated.

If we consider non-absorbing atmospheres ($\omega_o = 1$) and separate the total downward flux $\tilde{F}_-$ into a direct solar component F_d and a diffuse downward flux F_- then we again have a conservation relation,

$$A + (1-\rho)F_d + (1-\rho)F_- = 1 \tag{57}$$

As in the other diagram this relation can also be represented by points within an equilateral triangle. It is illustrated in Fig. 17 wherein any non-absorbing planetary atmosphere system can be represented. Thin atmospheres with low surface albedos are represented by points in the lower right corner of the triangle; thick atmospheres with low surface albedos have points along the left side of the triangle, and systems with high surface albedos are represented by points in the upper corner of the triangle. Using the radiative-transfer formulas I have calculated these components for various planetary systems with optical thickness ranging from a Rayleigh optical thickness to multiples thereof as high as 100. These cases are illustrated in Fig. 18.

5.3 Albedo-Radiance Relationship

Using the atmospheric-radiative-transfer model we can calculate the total albedo as a function of the total radiance. Such a relationship is more nearly consistent with an actual measurement of radiation by a satellite. Figure 19 illustrates the dependence of total albedo on the total spectral radiance in the vertical direction at the top of the atmosphere. Thirty-six planetary systems are represented, i.e. six surface albedos and six atmospheric states beginning with a pure Rayleigh atmosphere.

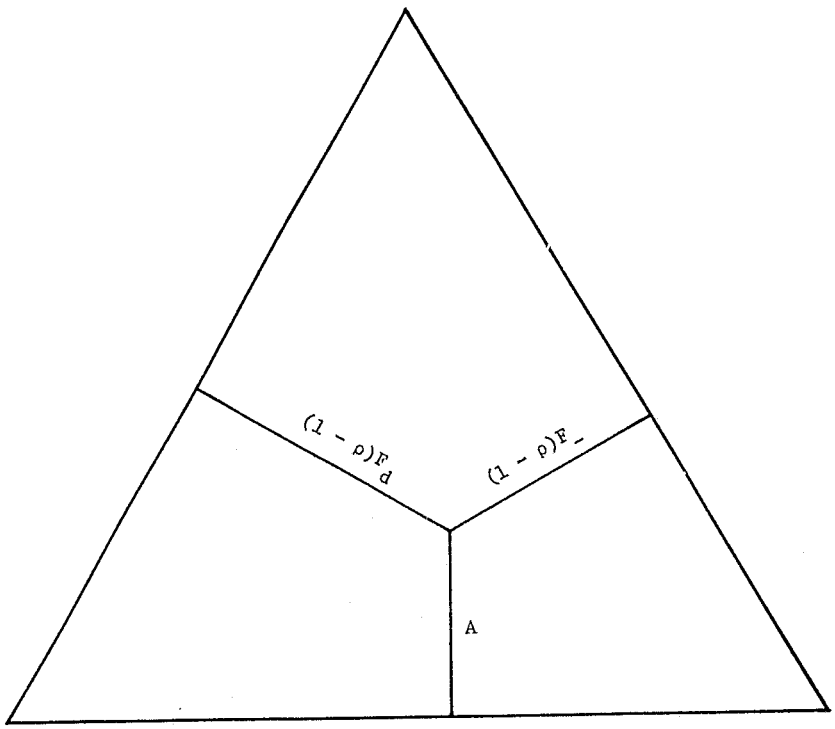

FIGURE 17
ENERGY CONSERVATION RELATION FOR
A NON-ABSORBING PLANETARY
ATMOSPHERE

A ∿ Total Albedo

$(1 - \rho)F_d$ ∿ Direct Flux Loss

$(1 - \rho)F_-$ ∿ Diffuse Flux Loss

FIGURE 18
RELATIONSHIP OF TOTAL ALBEDO, DOWNWARD DIRECT FLUX LOSS RATIO, AND DOWNWARD DIFFUSE FLUX LOSS RATIO FOR ATMOSPHERES WITH NO ABSORPTION. SOLAR ZENITH ANGLE = 30°; WAVELENGTH = 0.45 μm.

↑ - RAYLEIGH ATMOSPHERE

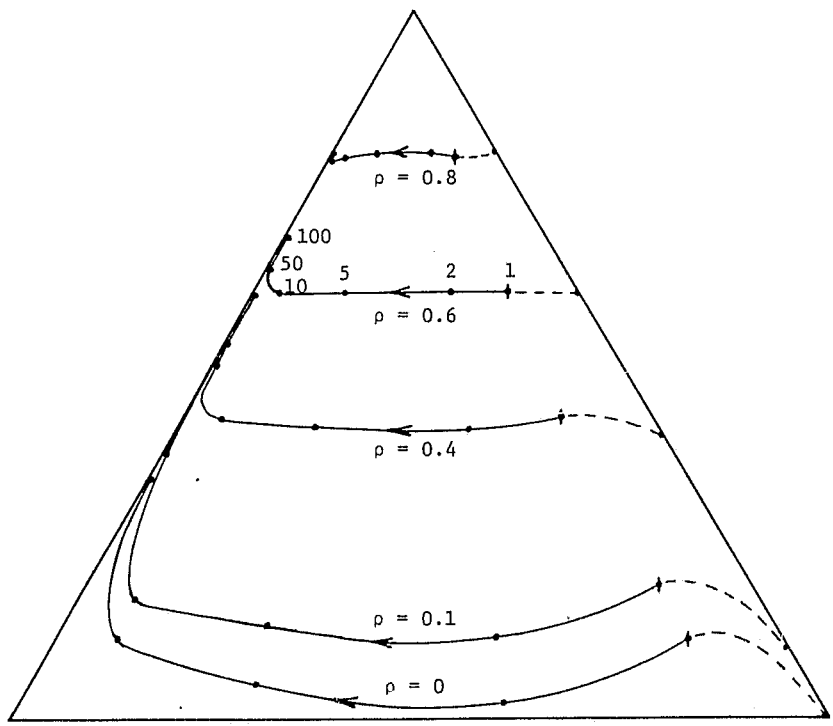

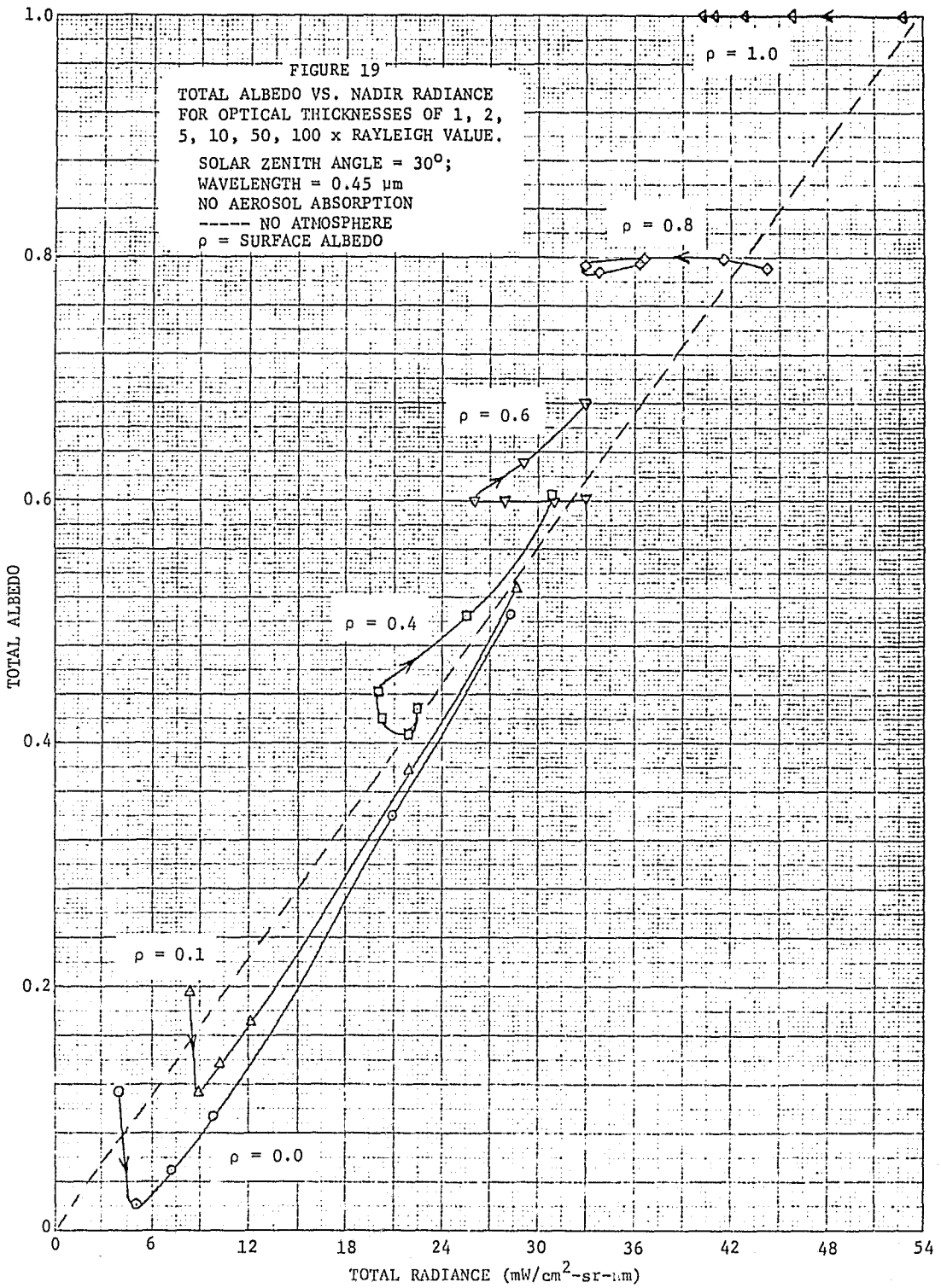
FIGURE 19
TOTAL ALBEDO VS. NADIR RADIANCE FOR OPTICAL THICKNESSES OF 1, 2, 5, 10, 50, 100 x RAYLEIGH VALUE.
SOLAR ZENITH ANGLE = 30°;
WAVELENGTH = 0.45 μm
NO AEROSOL ABSORPTION
----- NO ATMOSPHERE
ρ = SURFACE ALBEDO
ρ = 1.0
ρ = 0.8
ρ = 0.6
ρ = 0.4
ρ = 0.1
ρ = 0.0
TOTAL ALBEDO
TOTAL RADIANCE (mW/cm²-sr-μm)
0
0.2
0.4
0.6
0.8
1.0
0
6
12
18
24
30
36
42
48
54

The arrow on each line indicates the progression from a Rayleigh to an extremely dense atmosphere. It should be noted that the relationship is by no means a simple one; the complexities involve the competing effects of surface albedo and atmospheric turbidity. It does demonstrate, however, that given the surface albedo and the radiance the total albedo can be determined.

Another interesting relationship is the connection between total albedo and sky radiance. This is especially useful if a satellite or aircraft measurement is not feasible. The dependence of total albedo on vertical sky radiance is illustrated in Fig. 20.

5.4 Albedo-Irradiance Relationship

One of the easiest measurements to perform is that of the total irradiance at the surface. A flat-plate device will receive radiation from the entire hemisphere and include the direct solar as well as the downward diffuse irradiance. Again, model calculations were made to show the relationship between total irradiance and total albedo. This is illustrated in Fig. 21. The Rayleigh atmosphere is designated by the letter R. Thus, we see that for a given surface albedo and a measure of the total irradiance the total albedo can be determined.

A similar relationship exists between the diffuse sky irradiance and total albedo. This effect is illustrated in Fig. 22. In this case and in the preceding case it should be noted that there is a linear relationship between the total albedo and irradiance. The diffuse component of the flux is more difficult to measure since it requires that the sun be blocked out of the hemispherical field of view.

5.5 Total Albedo-Surface Albedo Relationship

Finally, we should understand the relationship between the total albedo and the surface albedo. The connection between the two is depicted in Fig. 23 in which the straight line represents zero optical thickness or no atmosphere. It should be noted that as the optical thickness of the atmosphere increases the total albedo decreases for a given surface albedo.

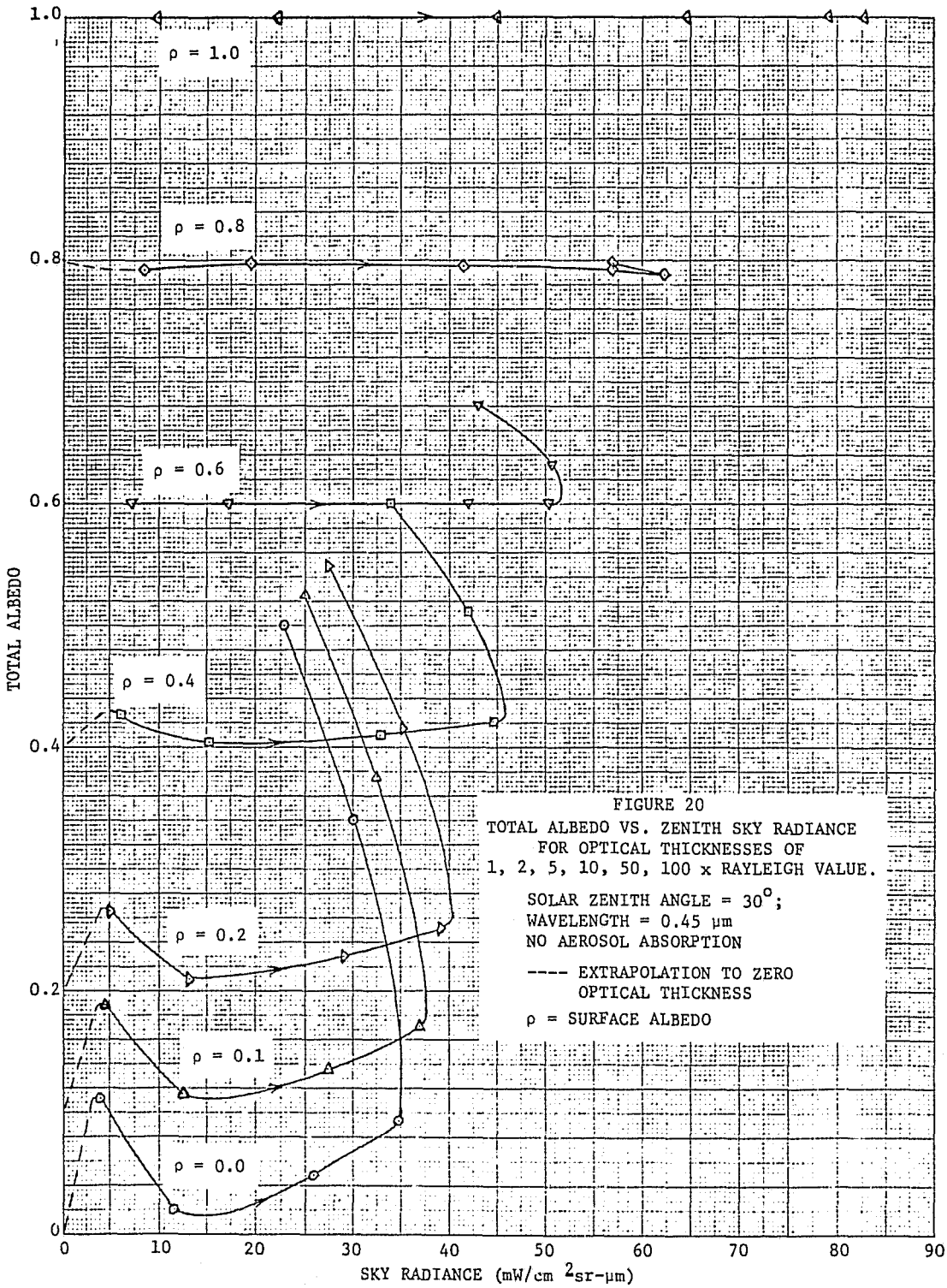

FIGURE 20
TOTAL ALBEDO VS. ZENITH SKY RADIANCE FOR OPTICAL THICKNESSES OF 1, 2, 5, 10, 50, 100 x RAYLEIGH VALUE.

SOLAR ZENITH ANGLE = 30°;
WAVELENGTH = 0.45 μm
NO AEROSOL ABSORPTION

---- EXTRAPOLATION TO ZERO OPTICAL THICKNESS

ρ = SURFACE ALBEDO

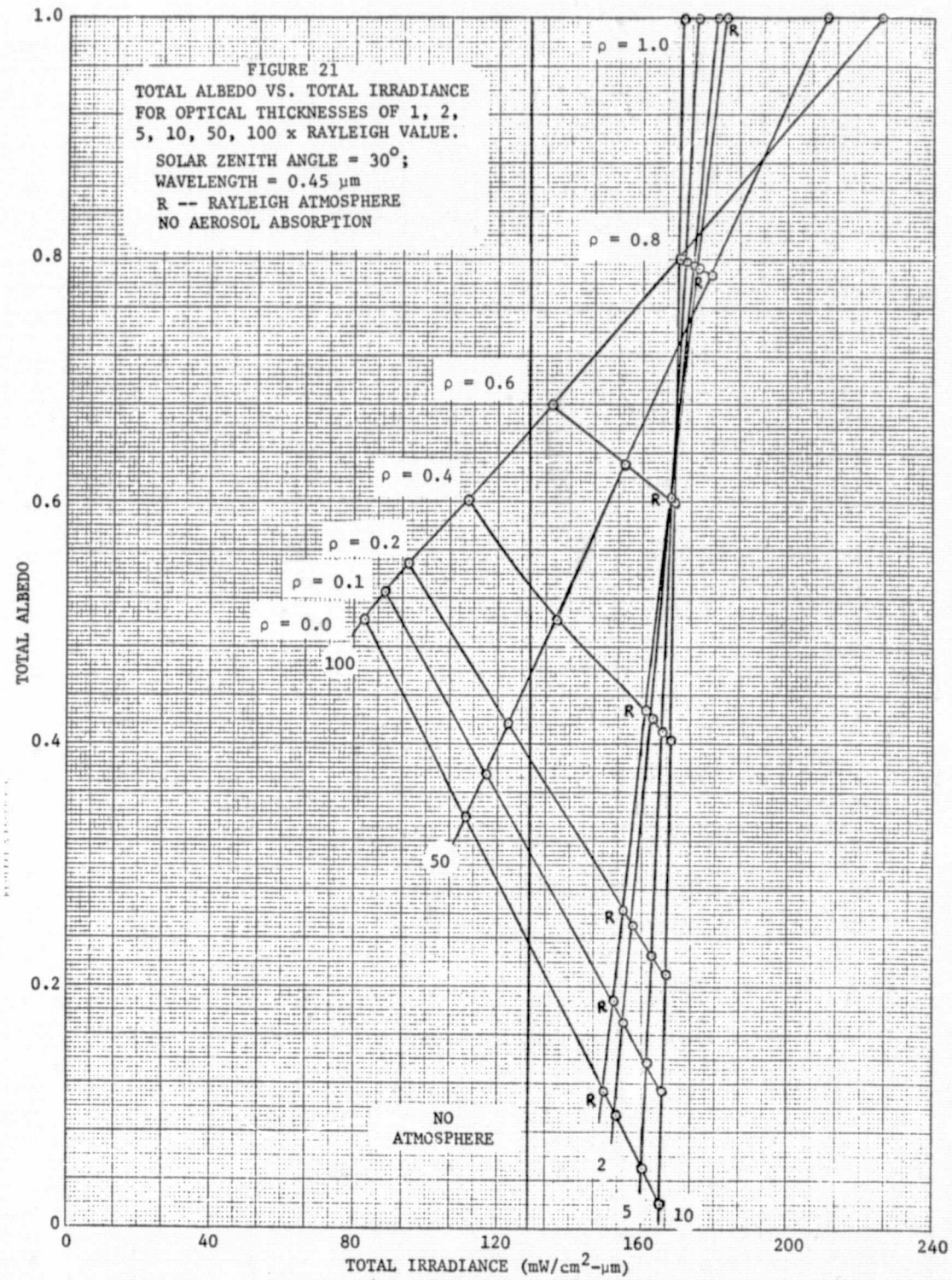
FIGURE 21
TOTAL ALBEDO VS. TOTAL IRRADIANCE FOR OPTICAL THICKNESSES OF 1, 2, 5, 10, 50, 100 x RAYLEIGH VALUE.
SOLAR ZENITH ANGLE = 30°;
WAVELENGTH = 0.45 μm
R -- RAYLEIGH ATMOSPHERE
NO AEROSOL ABSORPTION
ρ = 1.0
ρ = 0.8
ρ = 0.6
ρ = 0.4
ρ = 0.2
ρ = 0.1
ρ = 0.0
100
50
2
5
10
R
NO ATMOSPHERE
TOTAL ALBEDO
TOTAL IRRADIANCE (mW/cm²-μm)
0
0.2
0.4
0.6
0.8
1.0
0
40
80
120
160
200
240

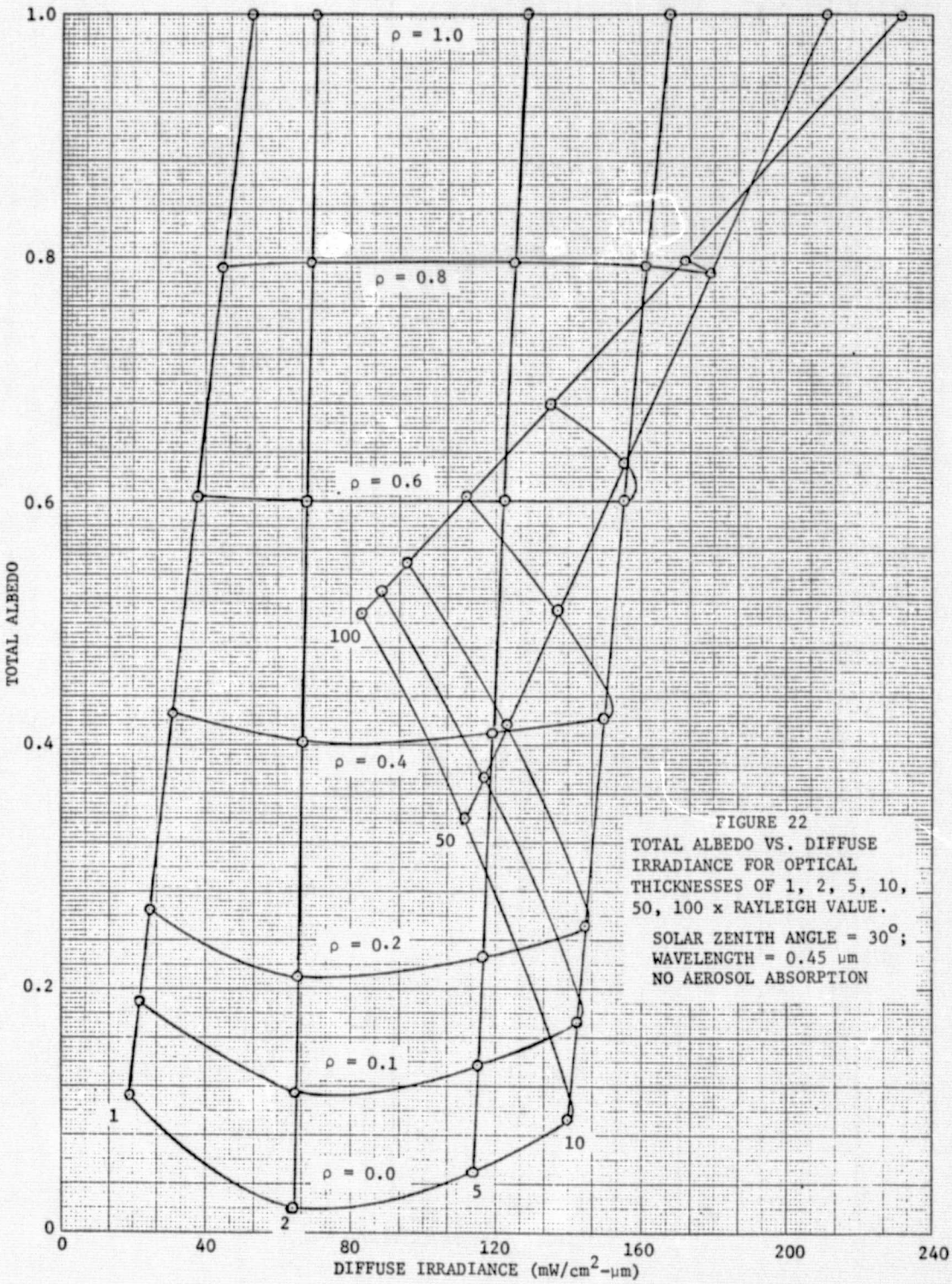

FIGURE 22
TOTAL ALBEDO VS. DIFFUSE IRRADIANCE FOR OPTICAL THICKNESSES OF 1, 2, 5, 10, 50, 100 x RAYLEIGH VALUE.
SOLAR ZENITH ANGLE = 30°;
WAVELENGTH = 0.45 μm
NO AEROSOL ABSORPTION

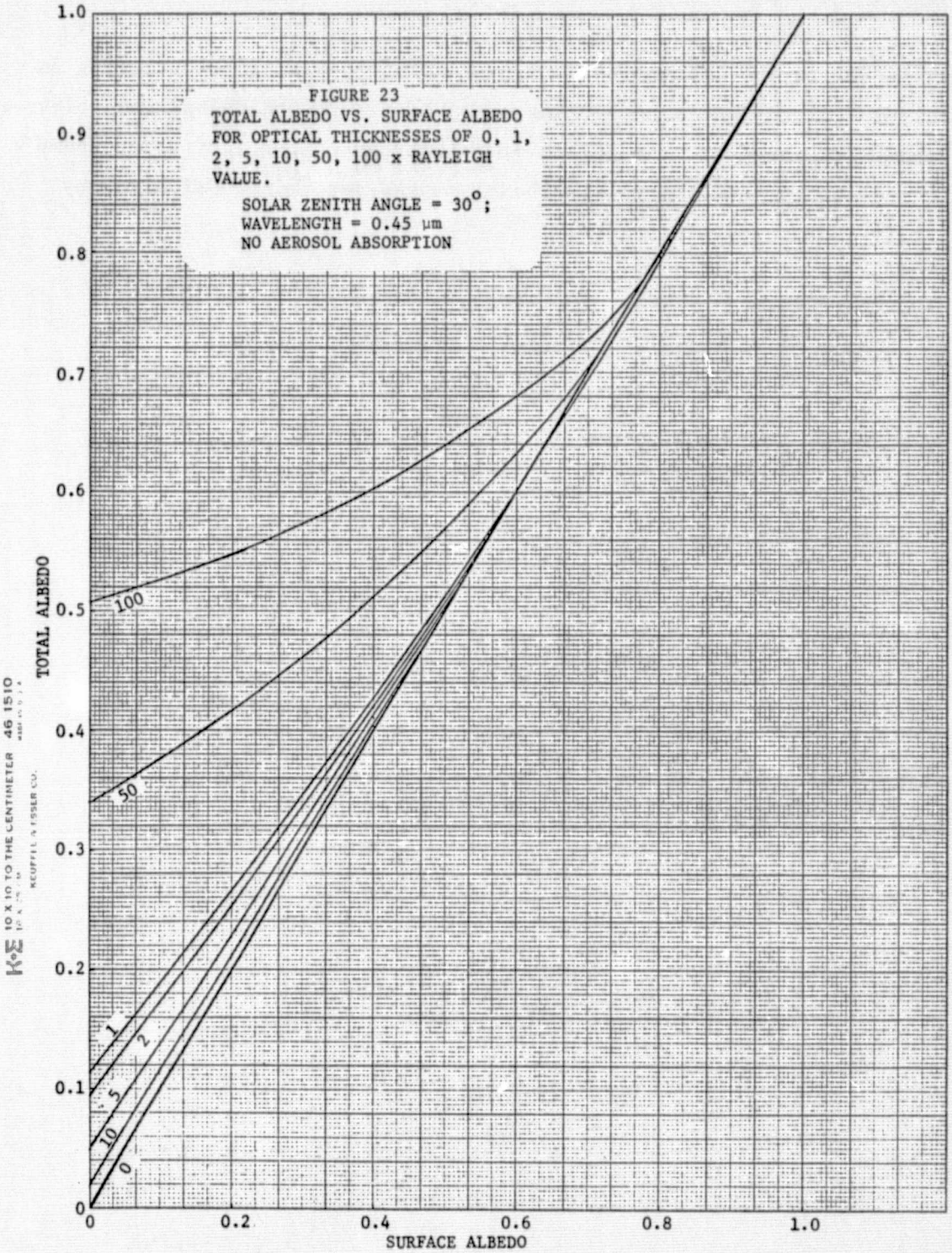

FIGURE 23
TOTAL ALBEDO VS. SURFACE ALBEDO FOR OPTICAL THICKNESSES OF 0, 1, 2, 5, 10, 50, 100 x RAYLEIGH VALUE.
SOLAR ZENITH ANGLE = 30°;
WAVELENGTH = 0.45 μm
NO AEROSOL ABSORPTION

This is due to the increasing degree of anisotropy of the scattering as more particulates are added to the atmosphere. Beyond an optical thickness of about $10\tau_R$ however, the degree of anisotropy of the scattering seems to have less effect and the total albedo is then determined primarily by the ever-increasing atmosphere.

6

Experimental Data

In this chapter we shall analyze the actual data obtained by SKYLAB and by other auxiliary means and make comparisons with the theoretical models.

6.1 SKYLAB Data

In this section we shall examine the SKYLAB data. The optimum site conditions for this investigation would have been to have a well-documented data collection area in or around the target area. The target and background should ideally be black so as to reduce the direct influence of the surface. Thus, the remote sensing equation would read

$$L = L_p \tag{58}$$

i.e. we have only the atmospheric path radiance to consider. Unfortunately, the real world does not have zero reflectance surfaces. During the first SKYLAB mission it was planned that data would be collected by the S-192 multispectral scanner over Pisgah Crater in California, a region with a very low surface reflectance. Difficulties with the original SKYLAB precluded this site however and the White Sands, New Mexico, site was chosen instead. On another SKYLAB mission we were able to get multispectral data for the Lake Michigan site.

6.1.1 White Sands, New Mexico

I chose two specific sites in the White Sands area. One was in the southern part of the bright White Sands area near Lake Lucero. The other was in the southern-most point of the lava flow and is representative of a region with a low surface albedo. These will be referred to as White Sands Bright and White Sands Dark respectively. The sites were chosen by

looking at SKYLAB photographic data in order to find a cloud-free area. From an account of the weather at the time SKYLAB flew over this particular site it was learned that some clouds were present, a fact which was not obvious upon detailed examination of the photographic data. It is easy to confuse bright sandy areas with clouds.

6.1.2 Lake Michigan

Another site which I chose was Lake Michigan under clear skies and in the deep-water area. The particular region chosen was about 10 miles west of St. Joseph, Michigan near the southern tip of the lake. At the time of the SKYLAB data take there were some clouds along the shoreline but the target area was clear. Besides the SKYLAB multispectral data we also had an aircraft overflight using the multispectral scanner aboard the ERIM-owned aircraft. In addition, the plane had an integrating nephelometer on board which sampled the air to collect data on the volume extinction coefficient.

6.2 Model Comparisons

We can now look at the absolute radiance values and compare the experimental results with our theoretical calculations.

6.2.1 White Sands, New Mexico

The specific White Sands National Monument consists of several hundred square miles of nearly pure gypsum ($CaSO_4 \cdot 2H_2O$) and because of its extensive area and high reflectance it is clearly visible at spacecraft altitudes. Careful measurements have been made of the spectral reflectance of specific regions in the White Sands area by Lindberg and Smith[36] who are permanently employed in the site area. The spectra for a sample of white sand, playa crust, and basalt are illustrated in Fig. 24. These spectra were used in the model comparison. Table II lists the S-192 bands, the corresponding wavelengths of the band centers, the spectral reflectance of white sand, the SKYLAB radiances, the experimental standard deviation, and the theoretical value of radiance as calculated from the radiative-transfer model. The model atmosphere chosen was a pure Rayleigh atmosphere

TABLE II. COMPARISON OF SKYLAB DATA WITH MODEL FOR THE WHITE SANDS (Bright) AREA.

Date: 14 June 1973 ; GMT: 14:44:46 ; Solar Zenith Angle: 32°28'54.5" ; Nadir View Angle: 5°32' ; Azimuth Angle: 47°6'36" ; Base Altitude: 1.2393 km

Band Number	Wavelength (μm)	Surface Reflectance (%)	SKYLAB Radiance (mW/cm^2-sr-μm)	Standard Deviation	Model Radiance (mW/cm^2-sr-μm)
1	0.4335	55.0	5.873	0.3426	23.84
2	0.4770	60.0	10.515	0.4458	32.23
3	0.5250	62.5	11.959	0.8167	30.23
4	0.5700	67.5	17.473	1.648	30.17
5	0.6265	70.5	13.894	0.7837	29.09
6	0.6940	71.0	10.968	0.4972	25.71
7	0.8300	73.0	9.341	0.4957	19.54
8	0.9900	70.0	5.087	0.2262	13.93
9	1.1100	74.0	2.942	0.1169	11.17
10	1.2150	60.0	2.957	0.1380	7.34
11	1.6400	52.0	1.160	0.05514	3.08

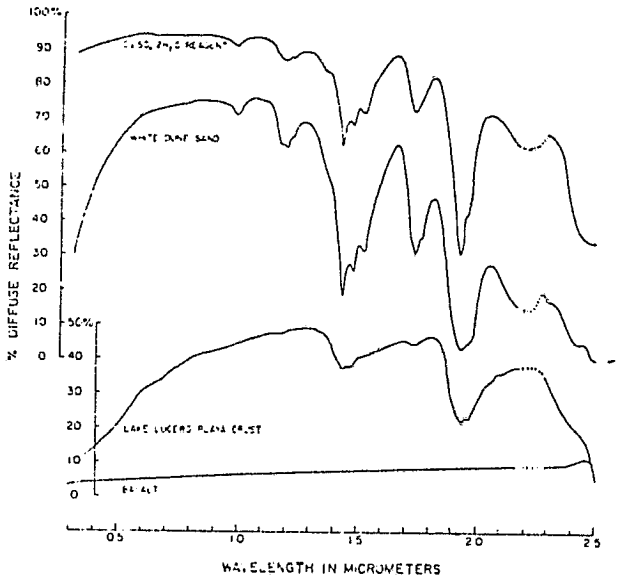

FIGURE 24. Diffuse reflectance spectra of reagent grade $CaSO_4 \cdot 2H_2O$ along with typical examples of white gypsum sand, Lake Lucero playa crust, and basalt. The curves have been smoothed to eliminate spectrophotometer noise and baseline effects.

which should give us the lowest radiance values. Instead, it should be noted that they are all consistently higher than the SKYLAB values by a factor of approximately three. This is illustrated in Fig. 25. How such a large discrepancy can exist is very puzzling. It is interesting that the ratio of theoretical-to-experimental values is nearly equal to pi. We took the theoretical radiances and divided them by pi and the experimental values. The spectrum is plotted in Fig. 26. Although there is a large fluctuation in the ratios the mean seems to be about 0.95. Could it be that the original calibration was off by a factor of pi? The experimental values were checked several times by individuals at ERIM who were thoroughly familiar with the SKYLAB multispectral calibration procedures and no discrepancy was indicated. I discussed the matter with Lawrence Korb now at the Goddard Spaceflight Center in Greenbelt, Md. He indicated to me

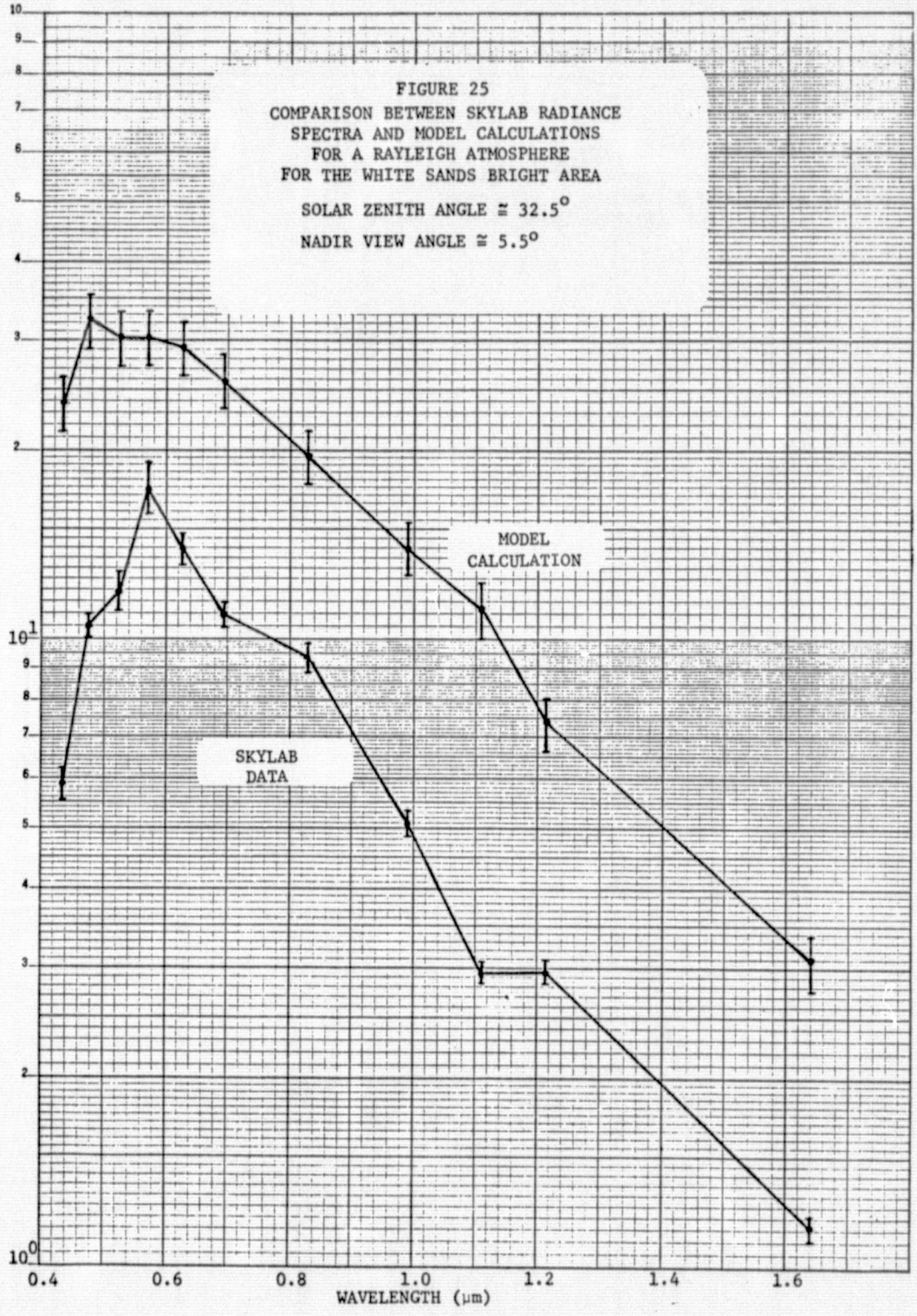
FIGURE 25
COMPARISON BETWEEN SKYLAB RADIANCE
SPECTRA AND MODEL CALCULATIONS
FOR A RAYLEIGH ATMOSPHERE
FOR THE WHITE SANDS BRIGHT AREA
SOLAR ZENITH ANGLE ≅ 32.5°
NADIR VIEW ANGLE ≅ 5.5°
MODEL CALCULATION
SKYLAB DATA
WAVELENGTH (μm)
0.4
0.6
0.8
1.0
1.2
1.4
1.6
10
9
8
7
6
5
4
3
2
10^1
10^0
K&E SEMI-LOGARITHMIC 46 4972
2 CYCLES X 70 DIVISIONS
KEUFFEL & ESSER CO.

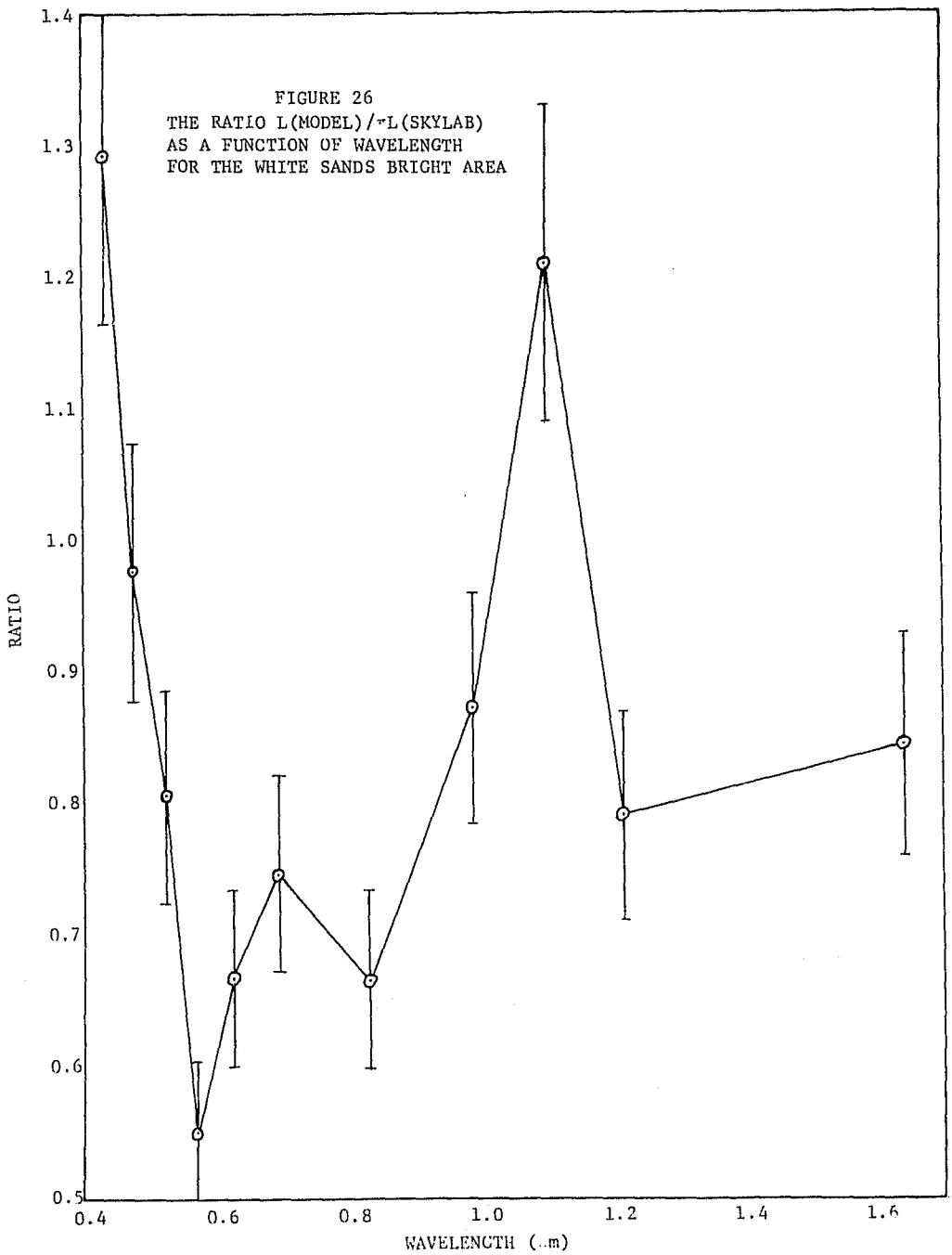

FIGURE 26
THE RATIO L(MODEL)/L(SKYLAB)
AS A FUNCTION OF WAVELENGTH
FOR THE WHITE SANDS BRIGHT AREA

that there were probably calibration problems somewhere. Is there any way of resolving the matter? If we include absorption in the model calculations it reduces the theoretical values by only a very small amount, certainly not enough to bring theory into agreement with experiment. Only an excessively large optical thickness could bring the two values into agreement as is illustrated in Fig. 27. It should be noted that by comparing the SKYLAB radiances in Table II with model extrapolation in Fig. 27 we would get optical thicknesses greater than 10, a completely unreasonable value. Is it possible that the model is incorrect? We have used this atmospheric-radiative-transfer model in conjunction with other experiments involving aircraft and LANDSAT data analysis and we have found no serious discrepancy. I have also compared the results of the model calculations with those of Coulson et al.[35] and the agreement is excellent. In addition, Coulson and Jacobowitz[37] calculated the radiance at the top of the atmosphere specifically for the White Sands area and got the same results that I did. Thus, there are three independent calculations of the spectral radiances which agree but which disagree with the SKYLAB values.

I have discussed the lack of agreement with J. Lindberg and E. Williamson both of the Atmospheric Sciences Laboratory at White Sands, N.M. Lindberg said his measurements have indicated an imaginary part of the particulate refractive index to be about 0.01 in the visible and near-infrared part of the spectrum, a value which is still too small by itself to decrease the theoretical values significantly. It was learned however, that it did rain in the site area prior to the SKYLAB data take and this could have reduced the surface albedo. It is possible that the reflectance could therefore be lower than the dry values by perhaps a factor of two. Thus, we conclude that only if the reflectance were reduced by an unreasonably large factor and the atmosphere at the time of the SKYLAB data take were strongly absorbing and optically very thick could there be agreement.

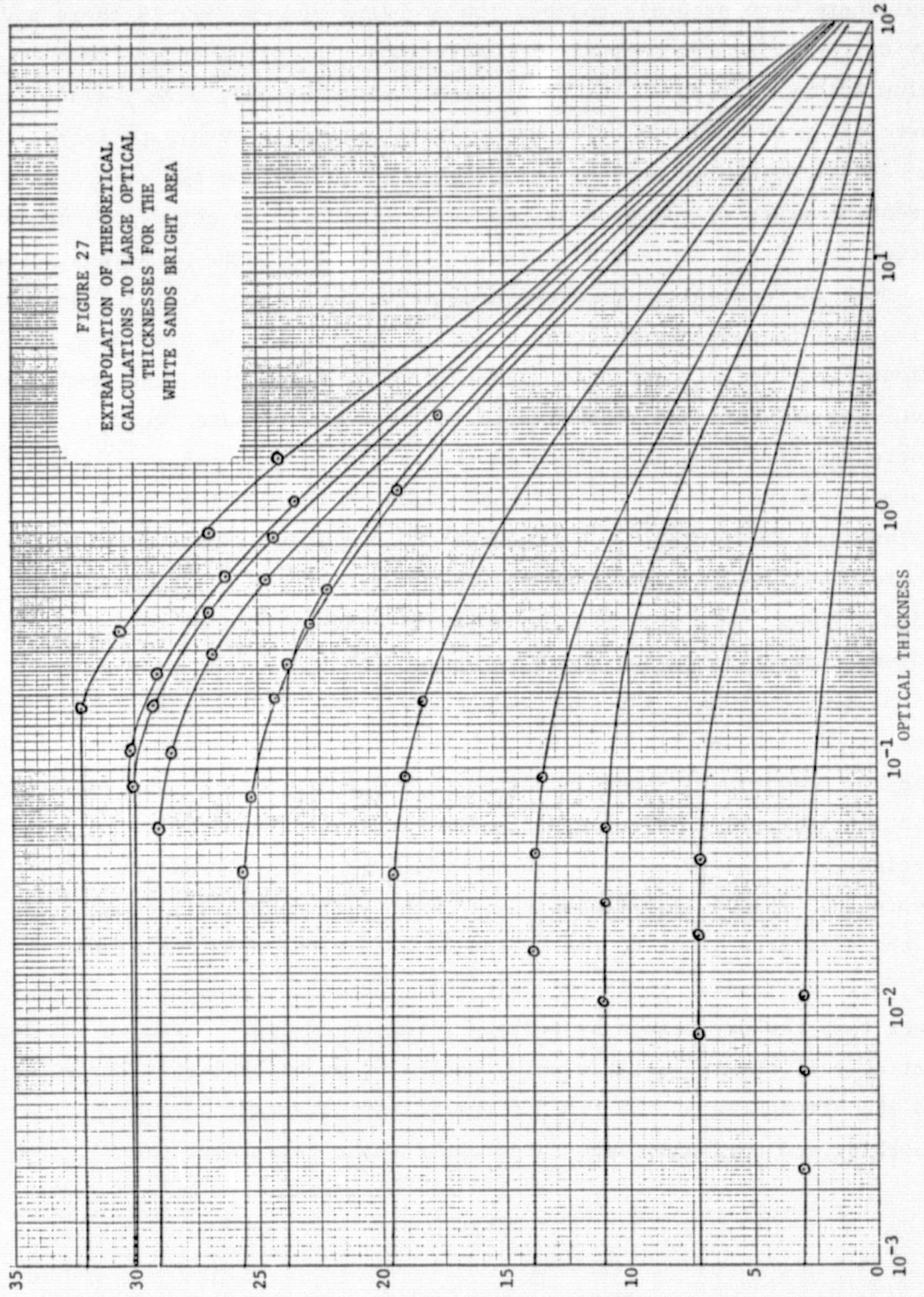
FIGURE 27
EXTRAPOLATION OF THEORETICAL CALCULATIONS TO LARGE OPTICAL THICKNESSES FOR THE WHITE SANDS BRIGHT AREA
35
30
25
20
15
10
5
0
10^{-3}
10^{-2}
10^{-1}
10^{0}
10^{1}
10^{2}
OPTICAL THICKNESS

We now turn to the analysis of SKYLAB data for the White Sands Dark area, i.e. the basalt region in the lava flow just north of the White Sands. Table III lists the comparisons between SKYLAB data and model calculations. A graphical display is depicted in Fig. 28. This time the model gives values about 1.5 times greater than the experimental radiance values and again it is difficult to see how they can be brought into agreement. It is true that wet basalt would have a reflectance smaller than the one used in the model calculations but not small enough to agree with experiment. Also, the lack of agreement seems to be about the same across the entire spectral region. We conclude that the same conditions prevail for this site as for the previous one.

6.2.2 Lake Michigan

Estimates of the reflectance of water are more difficult to make than for dry land as a result of the large temporal variations which can exist. The data which we chose were taken from measurements of Santa Monica by Wezernak[38]. A comparison of model calculations with SKYLAB data are listed in Table IV and a graph is illustrated in Fig. 29. Surprisingly, the agreement is much better than for the White Sands area although it should be noted that it is possible to make almost any theoretical calculation go through the experimental points. The experimental error is very large as can be seen in Fig. 29.

The ERIM multispectral scanner was flown over the site at almost the time of SKYLAB overpass and data were collected at three altitudes;

TABLE III. COMPARISON OF SKYLAB DATA WITH MODEL FOR THE WHITE SANDS (Dark) AREA.

Date: 14 June 1973 ; GMT: 14:44:42 ; Solar Zenith Angle: 32°20'7.25" ; Nadir View Angle: 5°32' ; Azimuth Angle: 24°52'9.623" ; Base Altitude: 1.280 km

Band Number	Wavelength (μm)	Surface Reflectance (%)	SKYLAB Radiance (mW/cm^2-sr-μm)	Standard Deviation	Model Radiance (mW/cm^2-sr μm)
1	0.4335	4.0	2.847	0.1959	4.954
2	0.4770	4.5	3.574	0.2190	5.171
3	0.5250	4.9	2.939	0.2885	4.065
4	0.5700	5.0	2.071	0.6202	3.368
5	0.6265	5.1	1.656	0.7079	2.823
6	0.6940	5.5	1.091	0.3422	2.408
7	0.8300	6.0	1.375	0.3518	1.770
8	0.9900	7.0	0.927	0.2636	1.453
9	1.1100	7.5	0.562	0.1372	1.162
10	1.2150	7.9	0.572	0.2015	0.985
11	1.6400	8.8	0.303	0.0811	0.524

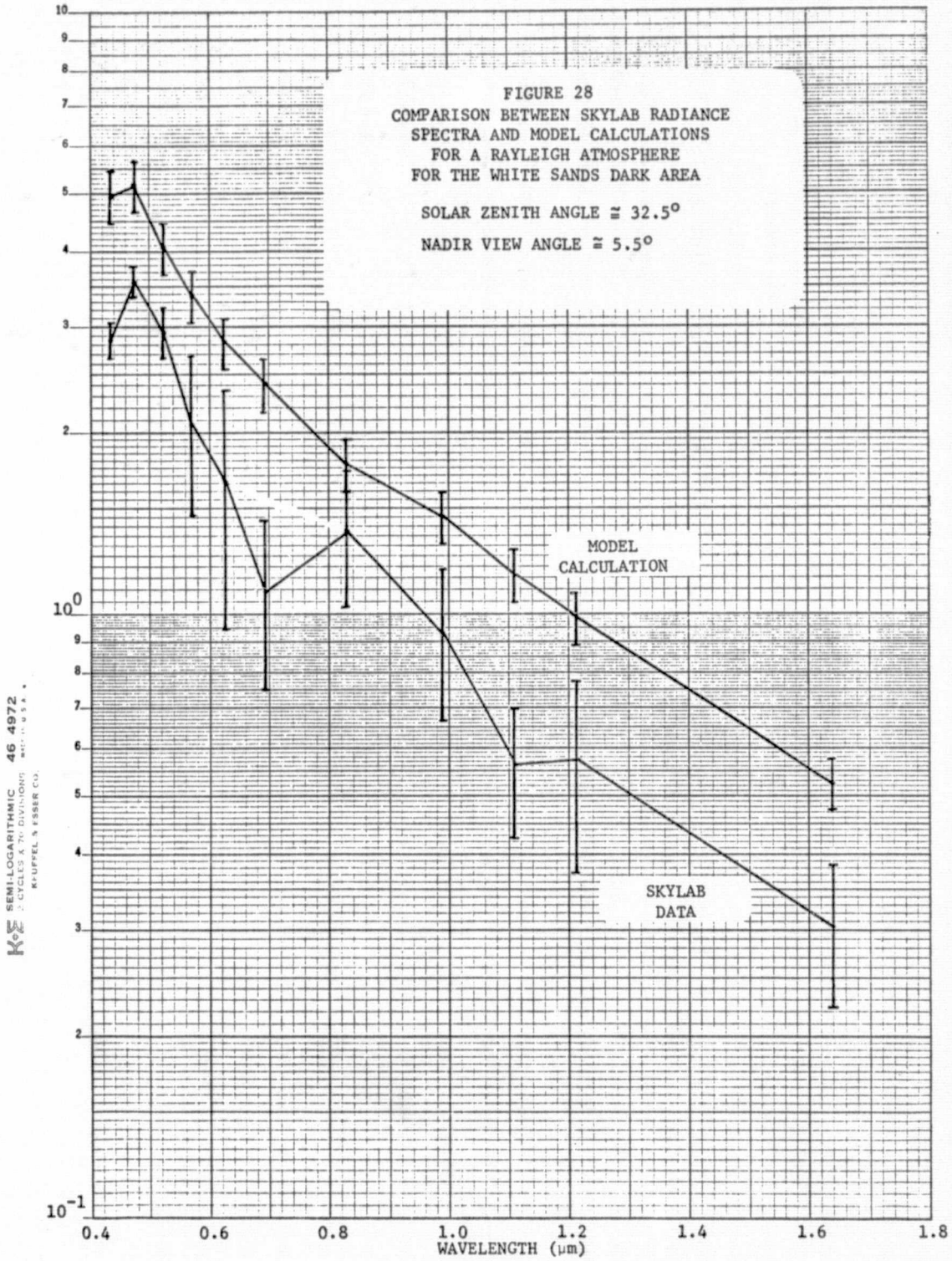
FIGURE 28
COMPARISON BETWEEN SKYLAB RADIANCE
SPECTRA AND MODEL CALCULATIONS
FOR A RAYLEIGH ATMOSPHERE
FOR THE WHITE SANDS DARK AREA
SOLAR ZENITH ANGLE ≅ 32.5°
NADIR VIEW ANGLE ≅ 5.5°
MODEL CALCULATION
SKYLAB DATA
10
9
8
7
6
5
4
3
2
10^0
9
8
7
6
5
4
3
2
10^-1
0.4
0.6
0.8
1.0
1.2
1.4
1.6
1.8
WAVELENGTH (μm)
SEMI-LOGARITHMIC
46 4972

TABLE IV. COMPARISON OF SKYLAB DATA WITH MODEL FOR THE LAKE MICHIGAN AREA.

Date: 18 Sept 1973 ; GMT: 16:00:11 ; Solar Zenith Angle: 43°41'13.25" ; Nadir View Angle: 5°32' ; Azimuth Angle: 102°48'17.039" ; Base Altitude: 0.177 km

Band Number	Wavelength (μm)	Surface Reflectance (%)	SKYLAB Radiance (mW/cm^2-sr-μm)	Standard Deviation	Model Radiance (mW/cm^2-sr-μm)
1	0.4335	3.4	3.107	0.1888	4.419
2	0.4770	2.6	4.630	0.1894	4.095
3	0.5250	2.35	3.849	0.2326	3.035
4	0.5700	1.9	5.488	0.3448	2.417
5	0.6265	1.6	1.252	0.4033	1.653
6	0.6940	1.3	0.5681	0.2258	0.971
7	0.8300	1.0	0.2979	0.2557	0.402
8	0.9900	0.5	0.1276	0.2337	0.149
9	1.1100	0.4	0.1095	0.1309	0.083
10	1.2150	0.3	0.0644	0.2331	0.049
11	1.6400	0.2	0.0197	0.1088	0.013

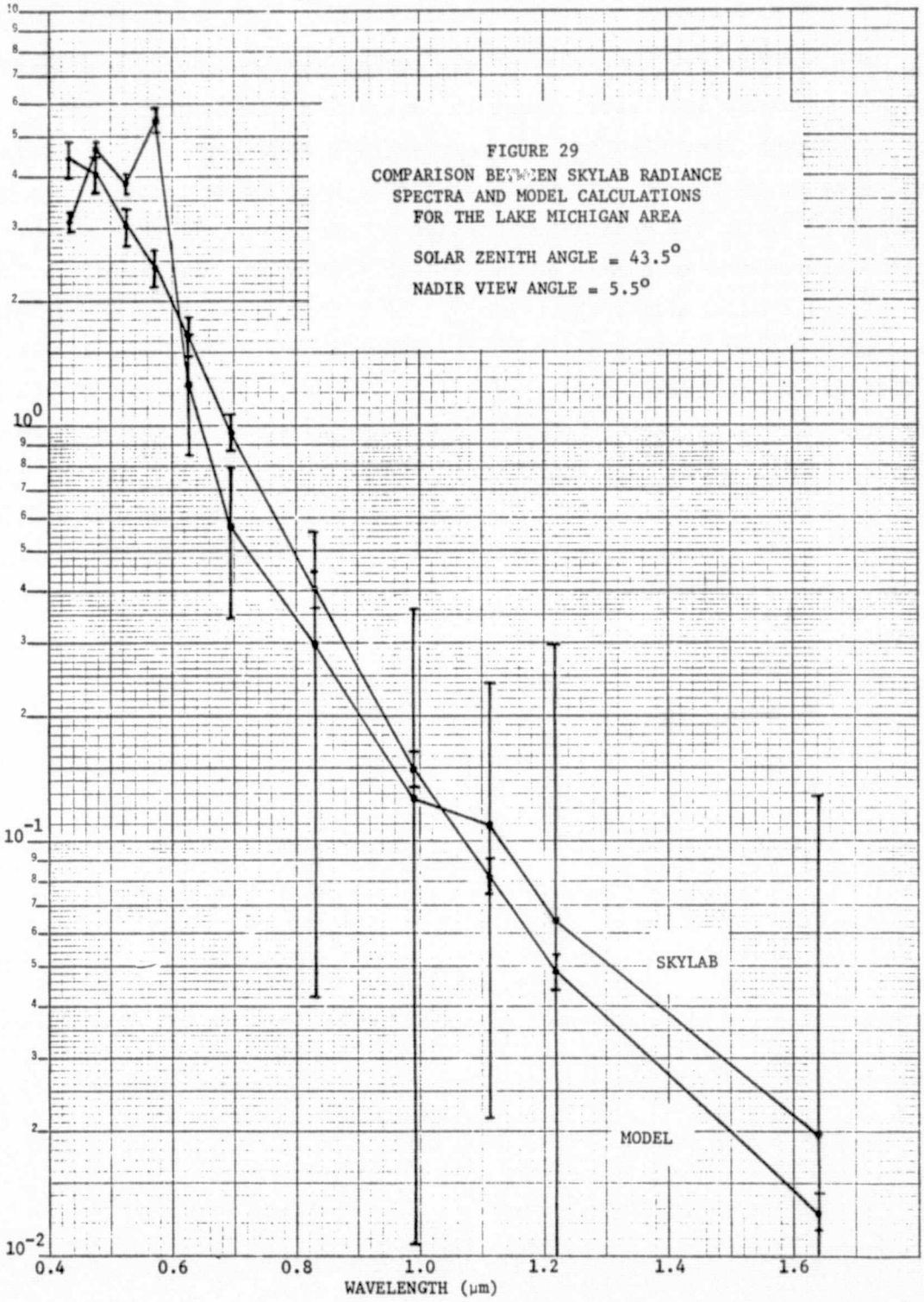

FIGURE 29
COMPARISON BETWEEN SKYLAB RADIANCE SPECTRA AND MODEL CALCULATIONS FOR THE LAKE MICHIGAN AREA

SOLAR ZENITH ANGLE = 43.5°

NADIR VIEW ANGLE = 5.5°

1000, 5000, 10,000 ft. These data with SKYLAB computations are plotted in Fig. 30. It is interesting that the spectra have almost the same spectral shape. They also become progressively larger in absolute radiance value as we go to higher altitudes, as should be. Unfortunately, one cannot say anything about the optical properties of the intervening atmosphere even though measurements were made of the volume extinction coefficient at the three aircraft altitudes. The reason is that the integrating nephelometer indicated a higher reading at 10,000 ft than it did at 5000 ft, a fact which is difficult to explain. Also, since there are no measurements at the surface or at altitudes greater than 10,000 ft there is no way that an optical thickness can be estimated. In the model calculations, we therefore assumed a pure Rayleigh atmosphere. Nevertheless, we also calculated the radiance assuming a small amount of absorption and the difference was very small.

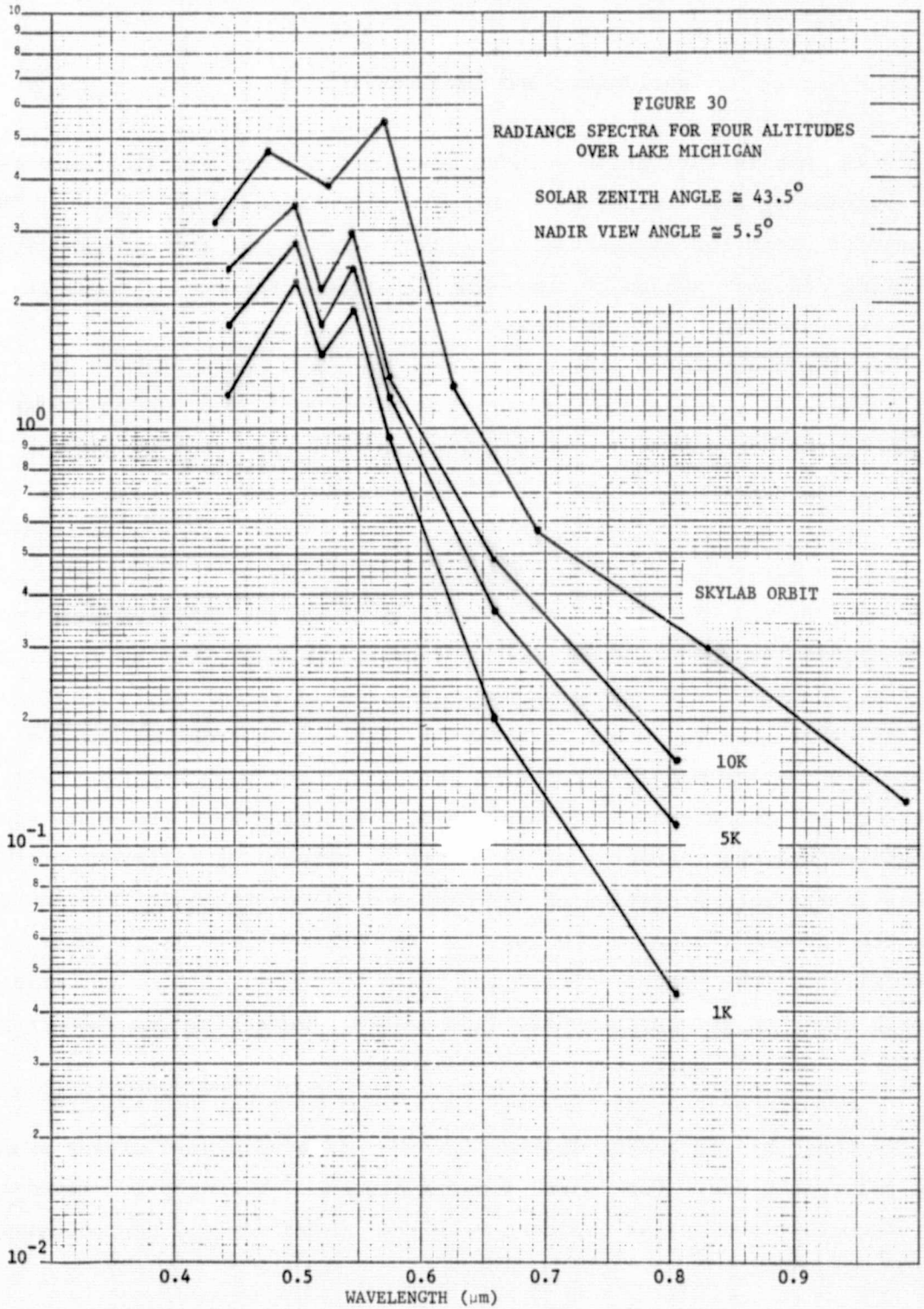
FIGURE 30
RADIANCE SPECTRA FOR FOUR ALTITUDES OVER LAKE MICHIGAN
SOLAR ZENITH ANGLE ≅ 43.5°
NADIR VIEW ANGLE ≅ 5.5°
SKYLAB ORBIT
10K
5K
1K
10^{0}
10^{-1}
10^{-2}
0.4
0.5
0.6
0.7
0.8
0.9
WAVELENGTH (μm)

7

Conclusions and Recommendations

In this investigation we have developed new and simple procedures for calculating and interpreting the spectral albedo of our planet. The triangular plots for the energy conservation relations are especially interesting and this method of representing atmospheric states shows promise for future studies of the atmospheres of planetary bodies.

Methods were also indicated whereby one can now perform simple measurements of various radiances and irradiances either at the top or bottom of the atmosphere and obtain knowledge of the total albedo.

It is unfortunate that the SKYLAB experimental data were unreliable. About the only thing which can be said is that spectrally these data did seem to match the model calculations reasonably well. As indicated in Chapter 6, the SKYLAB radiances were all about one-third of the model calculations for the White Sands Bright area and about two-thirds the model calculations for the White Sands Dark area. This is extremely difficult to explain other than to assume that SKYLAB calibration problems existed. In order to bring any model calculation into agreement with experiment it is necessary to make unreasonable assumptions regarding both the state of the atmosphere and the character of the Earth's surface. A different problem exists in the interpretation of the SKYLAB data for the Lake Michigan site. Here the agreement seems to be good but the SKYLAB error is so large, especially for the longer wavelengths that one can fit almost any atmospheric state to the experimental data points. Nevertheless, the aircraft and SKYLAB data do agree very well spectrally.

In spite of the difficulties associated with the SKYLAB data, I do believe that this method of determining the spectral albedo of our planet is a reasonable one. For future investigations, I strongly recommend that the spacecraft sensors be calibrated in the laboratory and periodically in

orbit by comparing radiance values with measurements made at selected test sites. Careful weather records should be taken at the test sites and radiance and irradiance should be measured periodically to insure the environmental stability of the area. If ground measurements and spacecraft measurements are taken at the same time for many selected test sites and these measurements are repeated many times then more reasonable estimates could be made of the spectral albedo of Earth. Such a determination of the albedo of the Earth-Atmosphere system is more than of academic interest. Indeed, it may determine the fate of civilization on our planet.

Appendix I

We present here the solutions for the diffuse upward flux $E_+(\tau)$, the diffuse downward flux $E_-(\tau)$, and the total (direct solar plus diffuse) downward flux $\tilde{E}_-(\tau)$ for a multiple scattering and absorbing medium.

$$E_+(\tau) = \Gamma \left\{(1-\eta)\omega_o \sinh k(\tau_o-\tau) + \Delta\left[(1-\eta\omega_o)\sinh 2k\mu_o\tau + k\mu_o \cosh 2k\mu_o\tau\right]\right\}$$

$$E_-(\tau) = \Gamma \left\{(1-\eta\omega_o)\sinh k(\tau_o-\tau) + k\mu_o \cosh k(\tau_o-\tau) + \Delta(1-\eta)\omega_o \sinh 2k\mu_o\tau\right\}$$

$$- \mu_o E_o e^{-\tau/\mu_o}$$

$$\tilde{E}_-(\tau) = \Gamma \left\{(1-\eta\omega_o)\sinh k(\tau_o-\tau) + k\mu_o \cosh(\tau_o-\tau) + \Delta(1-\eta)\omega_o \sinh 2k\mu_o\tau\right\}$$

where

$$\Gamma = \frac{\mu_o E_o}{[(1-\eta\omega_o) \sinh k\tau_o + k\mu_o \cosh k\tau_o]}$$

$$\Delta = \frac{\rho\mu_o k}{[(1-\eta\omega_o) - \rho\omega_o(1-\eta)] \sinh 2k\mu_o\tau_o + k\mu_o \cosh 2k\mu_o\tau_o}$$

$$k = \frac{\sqrt{(1-\omega_o)(1+\omega_o-2\eta\omega_o)}}{\mu_o}$$

Appendix II

The solutions of the radiative-transfer equation for path radiance and sky radiance for a multiple-scattering and absorbing medium are as follows:

$$L_p(\tau,\mu,\phi) =$$

$$\Lambda\omega_o(1-\eta)\left\{\sinh k(\tau_o-\tau) + k\mu\left[e^{-(\tau_o-\tau)/\mu} - \cosh k(\tau_o-\tau)\right]\right\} p(\mu,\phi,\mu_o,\pi+\phi_o)$$

$$+ \Lambda\left\{(1-\eta\omega_o-k^2\mu_o\mu)\sinh k(\tau_o-\tau)\right\} p(\mu,\phi,-\mu_o,\phi_o)$$

$$+ \Lambda k\left[(1-\eta\omega_o)\mu-\mu_o\right]\left[e^{-(\tau_o-\tau)/\mu} - \cosh k(\tau_o-\tau)\right] p(\mu,\phi,-\mu_o,\phi_o)$$

$$+ \Phi\left[1 + 2(1-\omega_o)\mu\right]\left[1+\omega_o-2\eta\omega_o\right]\left[\sinh 2k\mu_o\tau - e^{-(\tau_o-\tau)/\mu}\sinh 2k\mu_o\tau_o\right]$$

$$+ k\mu_o\Phi\left[1 + 2(1+\omega_o-2\eta\omega_o)\mu\right]\left[\cosh 2k\mu_o\tau - e^{-(\tau_o-\tau)/\mu}\cosh 2k\mu_o\tau_o\right]$$

and

$$L_S(\tau,-\mu,\phi) =$$

$$\Lambda\omega_o(1-\eta)\left\{\sinh k(\tau_o-\tau) + k\mu\cosh k(\tau_o-\tau)\right\} p(-\mu,\phi,-\mu_o,\pi+\phi_o)$$

$$-\Lambda\omega_o(1-\eta)e^{-\tau/\mu}\left[\sinh k\tau_o + k\mu\cosh k\tau_o\right] p(-\mu,\phi,-\mu_o,\pi+\phi_o)$$

$$+\Lambda(1-\eta\omega_o + k^2\mu_o\mu)\left[\sinh k(\tau_o-\tau) - e^{-\tau/\mu}\sinh k\tau_o\right] p(-\mu,\phi,-\mu_o,\phi_o)$$

$$+\Lambda k\left[(1-\eta\omega_o)\mu + \mu_o\right]\left[\cosh k(\tau_o-\tau) - e^{-\tau/\mu}\cosh k\tau_o\right] p(-\mu,\phi,-\mu_o,\phi_o)$$

$$+ \Phi\left[1 - 2(1-\omega_o)\mu\right]\left[1 + \omega_o - 2\eta\omega_o\right]\sinh 2k\mu_o\tau$$

$$+k\mu_o\Phi\left[1 - 2(1+\omega_o-2\eta\omega_o)\mu\right]\left[\cosh 2k\mu_o\tau - e^{-\tau/\mu}\right]$$

$$\Lambda = \frac{\omega_o E_o}{4\pi\left[1-(k\mu)^2\right]\left[(1-\eta\omega_o)\ \sinh k\tau_o + k\mu_o \cosh k\tau_o\right]}$$

$$\Phi = \frac{2\omega_o \rho k\mu_o{}^2 E_o}{4\pi\left[1-(2k\mu_o\mu)^2\right]\left[(1-\eta\omega_o)\ \sinh k\tau_o + k\mu_o \cosh k\tau_o\right]} \times$$

$$\left\{k\mu_o \cosh 2k\mu_o\tau_o + \left[1-\rho\omega_o - (1-\rho)\eta\omega_o\right] \sinh 2k\mu_o\tau_o\right\}^{-1}$$

and,

$$k = \frac{\sqrt{(1-\omega_o)(1+\omega_o - 2\eta\omega_o)}}{\mu_o}$$

REFERENCES

1. A. J. Drummond, Recent Measurements of the Solar Radiation Incident on the Atmosphere, Space Research XI, Akademie-Verlog, Berlin, 1971.

2. S. T. Henderson, Daylight and its Spectrum, American Elsevier Publishing Company, Inc., New York, 1970.

3. J. C. Arvesen, R. N. Griffin, Jr., and B. D. Pearson, Jr., Determination of Extraterrestrial Solar Spectral Irradiance from a Research Aircraft, Applied Optics, Vol. 8, No. 11, Nov., 1969.

4. M. P. Thekaekara and A. J. Drummond, Standard Values for the Solar Constant and its Spectral Components, Nature Phys. Sci., Vol. 229, Jan. 4, 1971.

5. E. Pettit, Astrophysics, ed. by J. A. Hynek McGraw-Hill, New York, 1951.

6. G. M. Hidy and J. R. Brock, An Assessment of the Global Sources of Tropospheric Aerosols, Proceedings of the 2nd International Clean Air Congress, H. M. England and W. T. Beerg, (Eds.), 1971, pp. 1088-1097.

7. C. E. Junge, Air Chemistry and Radioactivity, Academic Press, 1963.

8. D. Deirmendjian, Electromagnetic Scattering on Spherical Polydispersions, American Elsevier Publishing Company, Inc., 1969.

9. R. E. Turner, Radiative Transfer in Real Atmospheres, Final Report, ERIM 190100-24-T, Environmental Research Institute of Michigan, July 1975.

10. L. Lorenz, Videnskab. Selskab. Skrifter, Vol. 6, 1890.

11. G. Mie, Ann. Physik, 25, p. 377, 1908.

12. J. A. Stratton, Electromagnetic Theory, McGraw-Hill, New York, 1941.

13. H. C. van de Hulst, Light Scattering by Small Particles, John Wiley and Sons, 1957.

14. M. Kerker, The Scattering of Light and Other Electromagnetic Radiation, Academic Press, 1969.

15. H. Koschmieder, Beitr. Phys. Freien Atm., Vol. 12, 1924.

16. R. Horvath, M. Spencer and R. Turner, Atmospheric Corrections and Simulation of Space-Acquired Remote Sensor Data: 0.4- to 1.0-μm Spectral Range, Final Report, WRL 10657-5-F, 1972.

17. L. Elterman, Vertical-Attenuation Model with Eight Surface Meteorological Ranges 2 to 13 Kilometers, AFCRL Report No. 70-0200, Air Force Cambridge Research Laboratories, Bedford, Massachusetts, March, 1970.

18. E. Raschke and W. R. Bandeen, The Radiation Balance of the Planet Earth from Radiation Measurements of the Satellite NIMBUS II, J. of App. Met., Vol. 9, 1970.

19. S. I. Rasool and S. H. Schneider, Atmospheric Carbon Dioxide and Aerosols: Effects of Large Increases on Global Climate: Science, Vol. 173, p. 138, 1971.

20. R. A. Reck, Aerosols and Polar Temperature Changes, Science, Vol. 188, p. 728, 1975.

21. V. Ramanathan, Greenhouse Effect Due to Chlorofluorocarbons: Climatic Implications, Science, Vol. 190, p. 50, 1975.

22. R. W. Preisendorfer, Radiative Transfer on Discrete Spaces, Pergamon Press, Oxford, 1965.

23. Target Signature Analysis Center: Data Compilation Eleventh Supplement, AFAL-TR-72-226, Vols. I, II, III, Willow Run Laboratories, The University of Michigan, October 1972.

24. V. Leeman, D. Earing, R. K. Vincent and S. Ladd, The NASA Earth Resources Spectral Information System: A Data Compilation, 31650-24-T, Willow Run Laboratories, The University of Michigan, May, 1971.

25. D. Anding, R. Kauth, and R. Turner, Atmospheric Effects on Infrared Multispectral Sensing of the Sea Temperature from Space, Final Report, 2676-6-F, The University of Michigan, 1970.

26. W. A. Malila, R. B. Crane, C. A. Omarzu, and R. E. Turner, Studies of Spectral Discrimination, 31650-22-T, Willow Run Laboratories, The University of Michigan, 1971.

27. R. E. Turner and M. M. Spencer, Atmospheric Model for Correction of Spacecraft Data, Proceedings of the Eighth International Symposium on Remote Sensing of Environment, Center for Remote Sensing Information and Analysis, Willow Run Laboratories, The University of Michigan, 1972.

28. R. E. Turner, Atmospheric Effects in Remote Sensing, Remote Sensing of Earth Resources, Vol. II., F. Shahrokhi, Ed., 1973.

29. R. E. Turner, Contaminated Atmospheres and Remote Sensing, Remote Sensing of Earth Resources, Vol. III, F. Shahrokhi, Ed., 1974.

30. R. E. Turner, Signature Variations Due to Atmospheric Effects, Proceedings of the Tenth International Symposium on Remote Sensing of Environment, Center for Remote Sensing Information and Analysis, Environmental Research Institute of Michigan, 1975.

31. R. E. Turner, W. A. Malila, R. F. Nalepka, and F. J. Thomson, Proceedings of the Society of Photo-Optical Instrumentation Engineers, Vol. 51, 1975.

32. A. J. LaRocca and R. E. Turner, An IRIA State-of-the-Art Report, 107600-10-T, Environmental Research Institute of Michigan, 1975.

33. R. E. Turner and P. F. Lambeck, Natural and Artifical Illumination in Optically Thick Atmospheres, Final Report, 108300-4-F, Environmental Research Institute of Michigan, 1975.

34. S. Chandrasekhar, Radiative Transfer, Dover Publications, 1960..

35. K. L. Coulson, J. V. Dave, and Z. Sekera, Tables Related to Radiation Emerging from a Planetary Atmosphere with Rayleigh Scattering, University of California Press, 1960.

36. J. D. Lindberg and M. S. Smith, Reflectance Spectra of Gypsum Sand from the White Sands National Monument and Basalt from a Nearby Lava Flow, Amer. Mineralogist, Vol. 58, pp. 1062-1064, 1973.

37. K. L. Coulson and H. Jacobowitz, Proposed Calibration Target for the Visible Channel of a Satellite Radiometer, NOAA Technical Report NESS62, U.S. Dept. of Commerce, Oct. 1972.

38. C. T. Wezernak, Environmental Research Institute of Michigan, private communication.